

# Chapter 1

## GRMHD simulations of accretion onto exotic compact objects

Héctor R. Olivares Sánchez, Prashant Kocherlakota, Carlos A. R. Herdeiro

**Abstract** Some of the extensions to general relativity and to the Standard Model of particle physics predict families of hypothetical compact objects, collectively known as exotic compact objects (ECOs). This category can be defined to encompass non-Kerr black holes both within and beyond general relativity, as well as horizonless compact objects such as boson stars. In order to model observational signatures and identify possible detections, it is crucial to understand the interaction between these objects and their surrounding medium, usually plasmas described by the equations of general relativistic magnetohydrodynamics (GRMHD). To this end, we review the existent literature on GRMHD simulations of accretion onto these objects. These cover a variety of objects and accretion patterns. We conclude by listing possible directions to continue exploring this relatively young field.

### 1.1 Introduction

Many of the effects from extensions to general relativity (GR) and the Standard Model of particle physics are expected to manifest in strong gravity environments,

---

Héctor R. Olivares Sánchez (✉)

Departamento de Matemática da Universidade de Aveiro and Centre for Research and Development in Mathematics and Applications (CIDMA), Campus de Santiago, 3810-193 Aveiro, Portugal, e-mail: [h.sanchez@ua.pt](mailto:h.sanchez@ua.pt)

Prashant Kocherlakota

Black Hole Initiative at Harvard University, 20 Garden St., Cambridge, MA 02138, USA  
Center for Astrophysics, Harvard & Smithsonian, 60 Garden St., Cambridge, MA 02138, USA  
e-mail: [pkocherlakota@fas.harvard.edu](mailto:pkocherlakota@fas.harvard.edu)

Carlos A. R. Herdeiro

Departamento de Matemática da Universidade de Aveiro and Centre for Research and Development in Mathematics and Applications (CIDMA), Campus de Santiago, 3810-193 Aveiro, Portugal, e-mail: [herdeiro@ua.pt](mailto:herdeiro@ua.pt)

and are directly linked to relativistically compact objects. In fact, some of them directly predict new families of hypothetical compact objects, collectively known as *exotic compact objects* (ECOs). The advances in observing technologies of the last decades, such as Very Long Baseline Interferometry (VLBI), gravitational wave (GW) detectors, and the possibility of multi-messenger astronomy, allow us to zoom into the environments of compact objects, with a great potential for new discoveries in astro- and fundamental physics. However, without a proper understanding of the interaction between these objects and their environments, we risk to misinterpret environmental effects as new fundamental physics, or to miss the opportunity to make important discoveries.

Most of the baryonic matter in the Universe is in the state of plasma, and in general can be well described by the equations of general relativistic magnetohydrodynamics (GRMHD). Understanding the observational properties of ECOs in realistic astrophysical environments is one of the motivations to perform GRMHD simulations of accretion onto these objects.

Although the field is still quite young, in this review we aim to encompass the existent literature featuring such simulations. We will include not only GRMHD simulations, but also simulations performed in pure general relativistic hydrodynamics (GRHD).

This chapter is organized as follows. In Section 1.2, we give an overview of some of the most interesting families of ECOs, as well as some pre-requisites for their consideration as viable models for compact objects in our Universe. Later, in Section 1.3, we discuss some important issues that is necessary to consider from the point of view of modeling before embarking in performing GRMHD simulations. An actual review of the results currently available in the literature is presented in Section 1.4. Finally, in Section 1.5 we conclude by giving some future perspectives on the field.

## 1.2 A view on the landscape of Exotic Compact Objects

The most compact objects in the Universe are now widely believed to be black holes (BHs). Under the *Kerr hypothesis*, moreover, they are believed to be well modelled by the vacuum BHs of GR [127, 86]. For a large part of their century-old history, however, BHs were speculative, or exotic, solutions of GR. Observational evidence [105] together with the (unexpected) theoretical robustness of these solutions [116, 147, 142], slowly established their case as physical objects, abundantly realized in the Cosmos. Yet, their subtle phenomenology together with the theoretical puzzles they introduce [112, 65, 7] invite us to ask if the astrophysical BH *candidates* are - all of them [70] - well modelled by the Kerr solution.

There are two qualitatively different departures from the Kerr hypothesis. The first way is that the astrophysical BHs candidates are in fact BHs, in the sense of GR, but not Kerr BHs. It is important to observe they could be either non-Kerr BHs in GR or beyond GR, as will be expanded below. The second way is that the astro-

physical BH candidates are not BHs; they are compact objects without a horizon. We shall call all such speculative, alternative, dark compact objects ECOs, encompassing both *non-Kerr BHs* and *horizonless ECOs*.

### 1.2.1 Theoretical robustness

Precise strong gravity observables, such as gravitational waves and BH imaging, are largely theory-driven: one needs theoretical templates in order to interpret the results. By the same token, one needs such templates for ECOs, if these are to be considered as contenders for the data and to allow a hypothetical detection.

Still, before embarking on the considerable task of obtaining precision phenomenological templates for a generic ECO model, the model should have surpassed several important theoretical criteria, making it worthy of the phenomenological endeavour.

The first criterion is that the ECO should arise in a consistent theoretical model. This does not require the model to be complete. GR, for instance, is not UV complete; but within its regime of validity it is self-consistent, in particular offering a well-posed Cauchy problem (the hyperbolicity issue) [29]. This is by no means guaranteed for an ECO model. It is elucidative to consider two examples of its failure. The first one is in GR with “matter”. Consider the “matter” to be a Proca field, which is appealing because it leads to a popular model of horizonless ECOs called Proca stars [23]. Including apparently innocuous self-interactions for the Proca field leads to a breakdown of hyperbolicity [31, 32, 30, 103]. The second one is in modified gravity. Consider Einstein-scalar-Gauss-Bonnet models, which are appealing within higher curvature models because the equations of motion are still second order. Additionally, it has known examples of interesting non-Kerr BHs [83, 87, 131, 50, 9, 46, 74, 17]. However, it was observed that there is a breakdown of hyperbolicity in dynamical evolutions, at least for some classes of scalar-curvature couplings [117].

The second criterion is that the ECO should be sufficiently stable, so that it could play a role in astrophysical processes. Establishing mode stability of a given ECO model may be rather challenging, especially beyond spherical symmetry. Moreover there may be even more subtle instabilities, possibly unseen in a mode stability analysis. One such pathology of recent interest in the context of horizonless ECOs is the *light ring instability*, or *trapping instability*. Light rings are circular, bound, photon orbits that generically exist around BHs [42]. They are closely connected to strong gravity phenomenology, such as the ringdown of a perturbed BH/ECO [25] and the BH shadow [44]. For horizonless ECOs that can emerge from an incomplete gravitational collapse in GR, when they become sufficiently compact to have light rings, these come in pairs [39]. Together with a light ring similar to that of Kerr BHs, that is associated to the aforementioned strong gravity phenomenology, there is a second light ring which, unless, the null energy condition is violated, is a stable, bound photon orbit. These stable orbits are potentially problematic; they form a potential well

that can trap modes of null fields (such as gravity), leading to a strong backreaction and thus a spacetime instability. It was argued that this instability is non-linear [85]; moreover, the instability was confirmed to have short time scales in concrete ECO models [41]. As such, this may be a generic issue with horizonless ECO models that have light rings and have a clear formation mechanism. Another possible cause of instability of rotating horizonless ECOs is the existence of an ergoregion [35]. It has been shown, however, that generically the existence of an ergoregion in horizonless ECOs is accompanied by light rings [58]; in other words, light rings arise first when making a spinning object compact, making their associated instability a more fundamental one.

A third and final criterion is that the ECO should have a formation mechanism. Non-Kerr BHs in GR or modified gravity may, in general, form by gravitational collapse, in appropriate circumstances. But the formation of horizonless ECOs may be more delicate. Popular models, such as gravastars [94], fuzzballs [93] or wormholes [102], have no clear, under control formation mechanism, that has been dynamically tested, even though some general principles may exist. By contrast, a model of horizonless ECOs with a tested formation mechanism is the family of bosonic stars, the mechanism being known as gravitational cooling [128]. Together with the established stability of some of these stars (in regions of their parameter space), this has made bosonic stars a popular model of horizonless ECOs.

### 1.2.2 Horizonless ECOs

Many models of horizonless ECOs have been proposed throughout the years - see the review [26]. They have had different motivations, not always to replace BHs and solve their aforementioned theoretical puzzles; some, in fact, co-exist with BHs. The latter have other motivations, that could be theoretical - such as geons [141], to model classical particles in field theory - or phenomenological - such as bosonic stars (see the review [92]) - that could relate to fuzzy dark matter [76]. Most of these, however, do not fulfil one or more of the above criteria. Whereas this does not prevent some phenomenological considerations, e.g. computing geodesics or imaging properties under some academic models, or even full GRMHD simulations on a fix background, their linear and (especially) non-linear dynamics is often still out of reach.

One exception in which dynamics is under control is the broad family of bosonic stars. These are lumps of a complex, massive scalar or vector field. The scalar stars, known as boson stars, have been known for over half a century [84, 123], although their rotating versions were only found much later [126, 143]. The vector stars, known as Proca stars, have only been constructed and studied over the last decade [23] - see also [68]. To be in the astrophysical BHs mass range, these stars - at least in the simplest models - must be composed by ultralight bosonic particles, in fact, as a Bose-Einstein condensate of very many such ultralight particles in the same quantum state. Their collapse into a BH is prevented from Heisenberg's

uncertainty principle, up to a (model dependent) maximal mass. They can form via gravitational cooling [128] and many models (static and spinning) have dynamically stable regions in the parameter space [92], even though some unexpected instabilities have been found as well [124, 73].

It is not surprising, therefore, that there is a considerable literature on strong gravity phenomenology of bosonic stars (by which we mean both the scalar and vector cases, collectively). In particular GRMHD simulations on the background of bosonic stars have been performed, as described below [109]. Since some of the models in [109] are not dynamically stable, this has led to exploring the imaging of other bosonic stars, within the program of the *imitation game*: assessing possible degeneracies in imaging properties between BHs and horizonless ECOs. In [71] it was observed that spherical Proca stars could produce an effective shadow, due to a special property of timelike circular orbits, that could quench the magnetorotational instability (MRI) driving matter inwards in an accretion disk, effectively creating a void of emitting matter near the centre of the star. It was even possible to find a Proca star for which this effective shadow is similar in size to that of a Schwarzschild BH with the same mass. Subsequently, however, it was found that such Proca star have an unexpected instability against non-spherical dynamics [73], undermining this model of a BH foil. Still, as a proof of principle, it would be interesting to understand if such void creating mechanism actually holds in a more complete GRMHD analysis.

Spinning Proca stars, on the other hand, are dynamically robust in their fundamental state [124]. It was observed that these stars have a peculiar structure of their timelike, equatorial, counter-rotating, circular orbits, with disconnected regions of stable orbits [49]. This has led to the suggestions that matter accumulated in the regions of such stable orbits could mimic some imaging features of BHs [130]: not only a shadow, but also fine features attributed to the existence of light rings, but in a spacetime without light rings - Fig. 1.1. Again, it would be interesting to test if such features are kept or washed way in a more realistic GRMHD analysis. For other imaging studies of bosonic stars and their comparison with BHs see e.g. [138, 47, 40, 122, 119, 120, 121].

### 1.2.3 Non-Kerr BHs

The spectrum of non-Kerr BHs both in GR and beyond GR is immense. Imaging properties of such ECOs are now a very popular subject with hundreds of models analysed in more or less academic setups. Again, however, restricting to ECOs abiding the above criteria narrows down significantly the space of models. But since most of imaging analyses rely simply on computing geodesics, this program can be pursued even if the model lacks a strong theoretical support. A broad conclusion is that for most models current observations of Sgr A\* and M87\* can only constraint part (if any at all) of the parameter space.

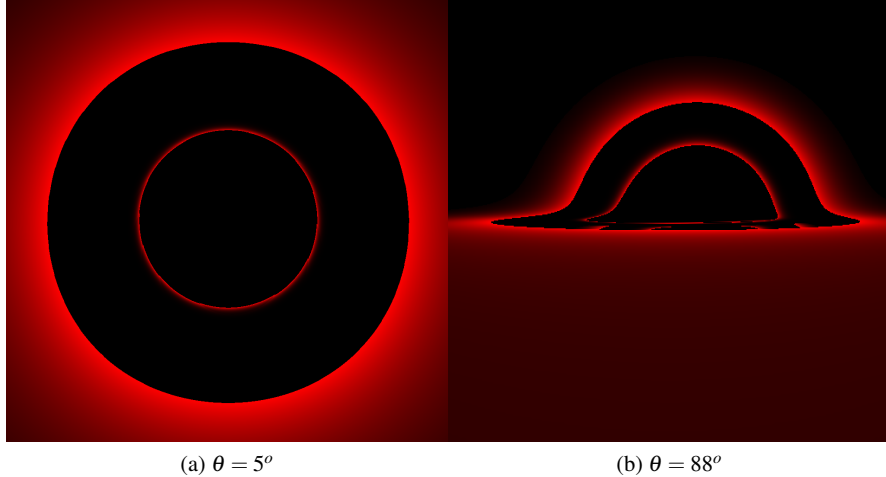


Fig. 1.1: Lensing images for a spinning Proca star without light rings but with discontinuous regions of equatorial, timelike circular orbits, wherein emitting matter is placed. The images are for two different co-latitude  $\theta$  observations. From [130].

GRMHD simulations, on the other hand, have been considered only for a handful of models. One case is dilatonic BHs [101, 118], which is a GR model, since the dilatonic (and axionic) field are minimally coupled to gravity, while non-minimally coupled to the electromagnetic field. These explorations support the expectation that in real-world observations imaging approaches will not be able to clearly distinguish such alternative models from Kerr using the current finite resolution of the EHT.

A similar conclusion can be found for many beyond GR models: the non-Kerrness is small and differences hard to tell from imaging e.g. [43, 46, 52]. But examples where dramatic differences from Kerr occur are also known. One such family is that of BHs with synchronised hair, which interpolates between Kerr BHs and spinning bosonic stars [72, 69]. Some dramatic imaging features can occur, such as chaotic lensing and multiple shadows of a single object [47]. In part of the parameter space such solutions have a natural formation mechanism via the phenomenon of superradiance [24], but in this region deviations from Kerr are smaller [45]. It would be quite interesting to perform GRMHD simulations on these backgrounds. In this respect, equilibrium configurations of self-gravitating accretion disks have been computed, which could be taken as initial data for such simulations [61, 62].

Let us comment that lensing has also been considered for even more exotic (and problematic) spacetimes, such as naked singularities [110, 82, 140]. Pushing GRMHD simulations on these background requires to face issues related to the arbitrariness of boundary conditions near the singularity, even though this may be mitigated for repulsive singularities. An interesting work performing GRHD simulations on a spacetime containing naked singularities can be found in Reference [16].

### 1.3 Practical considerations

In broad terms, the aim of a GRMHD simulation can be described as to increase the level of realism of a model for a relativistically compact object by modeling also its interactions with a surrounding medium. In most of the works based on GRMHD simulations of ECOs, the simulation data is further postprocessed to connect this modeling with observables.

During this process, physical models are transformed into numerical models, and it is crucial to ensure that, during this process, the essential features of physical models are preserved. This translates into making some choices for the numerical model, that are generally related to accommodating the physical model to the limitations of a numerical model. Here we briefly discuss a selection of these practical considerations, and some of the choices that require special attention when simulating ECOs surrounded by the interstellar medium.

*General assumptions.* All of the works reviewed in this chapter make the assumption that the fluid that makes the interstellar medium is non self-gravitating and its evolution does not back-react on the spacetime metric, so that the only source of gravity is the ECO. This is known as the *test fluid approximation*, and is justified for systems such X-ray binaries and supermassive black hole (SMBH) candidates, where the central object is several orders of magnitude more massive than the surrounding medium. In addition to this, the spacetime metric is not expected to evolve, so simulations are performed on *stationary spacetimes*. Other important assumptions are that the fluid is described by a gas with a simple equation of state (be it ideal or polytropic), and (for those involving magnetic fields), that it is a very good electric conductor. The latter is known as the *ideal magnetohydrodynamics* assumption, and it is generally an accurate description of interstellar plasmas. Finally, even though some of the ECOs that are simulated involve the presence of additional fields (general scalar, axion or dilaton fields), their couplings to the matter in the fluid or to the simulated electromagnetic field are ignored. Further comments on this assumption can be encountered in parts of Section 1.4 dealing with specific works in the literature .

*Flexibility to adopt custom metrics.* To simulate most of the ECO models described in Section 1.2, it is essential to endow GRMHD codes with the capability of performing covariant simulations on non-Kerr spacetimes. For analytic metrics, this just involves replacing the expressions for metric functions in the code by the appropriate ones. The applicability of this procedure can be significantly enlarged by the use of parameterized expansions, that can represent several theories by different values of the parameters [101, 104, 27, 28]. For cases where the metric is numerical (an important example are bosonic stars and BHs with synchronized hair), simulations may resort to tabulated metrics [108, 136] or to evaluations of spectral representations of the metric [97, 96].

*Initial conditions.* Due to the finiteness in time of numerical models, it is necessary to specify the configuration of the fluid at the start of the simulation. Naturally, this is problem-dependent, but we can mention here some generalities. Most of the simulations of magnetized accretion onto BHs and other compact objects start from

tori in hydrodynamic equilibrium to which magnetic loops are added. Even though these are the most widely used initial condition for this type of simulations, their applicability is limited to initially small magnetic fields, as their inclusion breaks this equilibrium [36]. Solutions for magnetized tori in true equilibrium have been obtained for boson stars and BHs with scalar hair in [61, 62], although they have so far not been utilized in simulations. In fact, the sub-field of equilibrium solutions in this kind of spacetimes features quite interesting results, that differ in significant ways from those that are possible around Kerr BHs (see e.g. [135, 134]).

*Boundary conditions.* We also need to specify the behavior of the fluid when interacting with the spatial boundaries of the simulation. Simulations of ECOs can present very different challenges to those of accretion onto Kerr BHs. For objects that possess an event horizon, it is customary to extend the simulation domain slightly inside it in order to prevent signals associated to the boundary from propagating into the simulation and producing spurious effects (see e.g. [37]). For this reason, it is important to use horizon penetrating expressions for the metric. These have been obtained for some general classes of metrics, and due to the importance of the subject, we have dedicated Section 1.3.1 to the procedure for obtaining them.

For the case of horizonless compact objects, there are two possibilities: either the simulation domain has a boundary at a physical surface, or it continues down to the center of the object. ECOs with surfaces have not been considered so far for GRMHD simulations, however there are works in the literature that simulate accretion onto objects with physical surfaces such as neutron stars (see Section 1.4.1). For cases where the center of the object is part of the computational domain, care must be taken to avoid problems related to the coordinate singularity at the origin of spherical coordinates. This can be done by selecting boundary conditions with the appropriate symmetry properties or by ensuring communication between neighboring cells at each side of the singularity [97, 109]. Another approach is to remove the coordinate singularity by resorting to Cartesian coordinate systems (see e.g. [96, 136]). The case of GRHD simulations in spacetimes with true curvature singularities was explored in [16]. Although the proper way to treat numerically domains that contain such singularities is still an open problem; one can consider (as argued by the authors of [16]) that a naked singularity is a pathology of classical GR which should be replaced by something else in a yet unknown full theory. This motivates setting, for instance, absorbing boundary conditions around the region containing the unknown physics, and excising it from the domain, as done in the cited work.

### 1.3.1 Horizon-Penetrating Coordinates

Most current codes used to perform GMRHD simulations require, reasonably, the spacetime metric in a horizon-penetrating form, to avoid numerical issues due to the presence of the coordinate singularity at the horizon. For the Kerr metric, specific coordinates, suitable for simulations, were introduced in Refs. [53, 95]. A large

class of geodesically-integrable, asymptotically-flat BH spacetimes, characterized by four free functions, were discovered in Ref. [77]. The horizon-penetrating Kerr-Schild form of such Johannsen(-Psaltis) spacetimes was also obtained there (Sec. V) and has recently been used to simulate accretion in such spacetimes [104, 28].

The horizon-penetrating form for yet another broad class of stationary and axisymmetric spacetimes was reported in Ref. [88]. The Azreg-Aïnou (AA) metric, used there, was discovered in Refs. [13, 11, 12] in an attempt to obtain stationary and axisymmetric solutions, through an algorithmic procedure similar to the one employed by Newman & Janis [107], from a static and spherically-symmetric “seed” metric. The AA metric has the value of describing null geodesically-integrable spacetimes, rigidly rotating BHs, and of capturing several well-known solutions to GR and alternative theories, some of which we discuss in Sec. 1.4.2 below.

We now briefly review the steps involved in arriving at coordinates that are suitable for GRMHD simulations, using the AA metric as a simple case study. Its line element in Boyer-Lindquist (BL; [22]) coordinates,  $x^\mu = (t, r, \vartheta, \varphi)$ , is given as [12, 88]

$$\begin{aligned} ds^2 = & \frac{X}{\Sigma} \left[ - \left( 1 - \frac{2F}{\Sigma} \right) dt^2 - 2 \left( \frac{2F}{\Sigma} \right) a \sin^2 \vartheta dt d\varphi + \frac{\Pi}{\Sigma} \sin^2 \vartheta d\varphi^2 \right. \\ & \left. + \frac{\Sigma}{\Delta} dr^2 + \Sigma d\vartheta^2 \right], \end{aligned} \quad (1.1)$$

where  $a$  denotes the spin parameter and the metric functions are not all independent. In addition to the conformal factor  $X$ , there are only two other free functions,  $A = A(r)$  and  $B = B(r)$ . The latter pair determines the remaining metric functions via  $2F = A - B$ ,  $\Delta = B + a^2$ ,  $\Sigma = A + a^2 \cos^2 \vartheta$ , and  $\Pi = (A + a^2)^2 - \Delta a^2 \sin^2 \vartheta$ .

To obtain the Kerr metric, one sets  $X = \Sigma$ ,  $A = r^2$ , and  $B = r^2 - 2Mr$ . For the Kerr-Newman metric [106], which is the stationary electrovacuum BH solution of the Einstein-Maxwell equations,  $B$  is modified to  $B = r^2 - 2Mr + Q^2$ . In the above,  $M$  and  $Q$  are the Arnowitt-Deser-Misner (ADM; [10]) mass and charge of the spacetime respectively.

When used to describe BH spacetimes, horizons are permitted at the roots of  $\Delta$ , where the  $rr$ -component of the metric diverges. This coordinate singularity can be eliminated by moving to coordinates,  $x^\mu = (\tau, r, \vartheta, \varphi)$ , in which the one-form field associated with the ingoing principal null congruence (PNC) of the spacetime,  $(\ell_-)_\mu = [-\Delta, -\Sigma, 0, \Delta a \sin^2 \vartheta]$ , becomes  $(\ell_-)_{\bar{\mu}} = [-1, -1, 0, a \sin^2 \vartheta]$ . The Jacobian,  $\Lambda^{\bar{\mu}}_\mu = \partial_\mu x^{\bar{\mu}}$ , for the desired transformation from BL to these so-called “spherical ingoing Kerr-Schild” (siKS) coordinates is given as

$$\Lambda^{\bar{\mu}}_\mu = \begin{bmatrix} 1 & 2F/\Delta & 0 & 0 \\ 0 & 1 & 0 & 0 \\ 0 & 0 & 1 & 0 \\ 0 & a/\Delta & 0 & 0 \end{bmatrix}. \quad (1.2)$$

The horizon-penetrating form of the metric (1.1) is then [88]

$$ds^2 = \frac{X}{\Sigma} \left[ - \left( 1 - \frac{2F}{\Sigma} \right) d\tau^2 + \left( 1 + \frac{2F}{\Sigma} \right) dr^2 + \Sigma d\vartheta^2 + \frac{\Pi}{\Sigma} \sin^2 \vartheta d\phi^2 - 2 \left( \frac{2F}{\Sigma} \right) a \sin^2 \vartheta d\tau d\phi + 2 \left( \frac{2F}{\Sigma} \right) d\tau dr - 2 \left( 1 + \frac{2F}{\Sigma} \right) a \sin^2 \vartheta dr d\phi \right], \quad (1.3)$$

from which we see that there are no divergences at the horizons ( $\Delta = 0$ ).

The two key ingredients therefore are finding both the 1-form field associated with the ingoing PNC in BL coordinates and the coordinate transformation that transforms it to an accepted standard form,  $(\ell_-)_{\bar{\mu}} = [-1, -1, 0, a \sin^2 \vartheta]$ . Thus, the siKS coordinates are adapted to the ingoing PNC in a specific way, and, thus, penetrate the future horizon. The metric above has recently been used to perform GRMHD simulations in “dilaton-axion” BH spacetimes, as discussed below in Sec. 1.4.2.3. Furthermore, the Jacobian (1.2) can be used to conveniently transform GRMHD data back to BL coordinates, if of interest.

The 3+1 split of the metric (1.3) has also been discussed in Ref. [88], from which it becomes clear that the fiducial choice for the congruence of hypersurface-forming Eulerian observers corresponds to a timelike one that has the same angular velocity as that of the zero angular momentum observer congruence.

It is worth noting that the closely-related set of spherical ingoing *null* Kerr-Schild coordinates,  $x^{\bar{\mu}} = (v, r, \vartheta, \phi)$ , more commonly used in the GR literature, are obtained by transforming the ingoing PNC generator to the form  $(\ell_-)_{\bar{\mu}} = [-1, 0, 0, a \sin^2 \vartheta]$ . From  $\ell_-^{\bar{\mu}} = -\delta_r^{\bar{\mu}}$ , we see that these are truly adapted to the ingoing PNC. For the Kerr metric, in particular, this form can be seen, e.g., in Sec. 5.3.6 of Ref. [113]. The Jacobian for the coordinate transformation from BL coordinates is similar to the one in eq. 1.2 with the term  $2F/\Delta$  being modified to  $2F/\Delta + 1$ .

## 1.4 GRMHD simulations of accretion onto exotic compact objects

### 1.4.1 Horizonless compact objects

Accretion onto compact objects with no event horizon is of particular interest, as it is expected to produce a qualitatively different phenomenology from that onto BHs, as matter does not disappear behind the event horizon. For compact objects with a surface, such as neutron stars, one would expect an interaction between this surface and the accreting matter, which should result in heating the surface. However, in practice, GRMHD simulations of accretion onto neutron stars employ absorbing boundary conditions [111] or simply remove the matter that falls onto the surface from the simulation [48]. Instead, the physics of the surface is usually accounted for in post-processing, at the stage of calculating images and spectra. For instance, [33] considers the cases of thermally emitting and reflecting surfaces. The results of

such analysis apply also to ECOs with surfaces for which the exterior metric is very close to that of Schwarzschild and Kerr BHs, such as gravastars.

More interesting from the point of view of GRMHD simulations are horizonless compact objects that also lack surfaces. Most of the literature on accretion onto this kind of objects refers to boson stars, although there exist at least one work simulating accretion onto Kerr superspinars (Section 1.4.1.4) and another one considering the case of wormholes (Section 1.4.1.5). Boson stars can be considered as surfaceless objects when the scalar field that constitutes them has very weak couplings with the particles of the standard model. In such case, the exotic object interacts with the accretion flow only through gravity, behaving as a clump of dark matter. A similar reasoning can be applied to other ECOs such as Proca stars; however, the available literature is limited to the simulation of accretion onto boson stars, likely due to the simplicity of their construction.

#### 1.4.1.1 Accretion-Ejection in boson stars

The earliest simulations are those of [97], which were performed in pure hydrodynamics using the code GR-AMRVAC. In such work, Meliani and collaborators explore different accretion scenarios onto boson star metrics generated by the spectral solver KADATH [64] for the case of a free scalar field (no self-interaction), that is, subject to the potential

$$U(|\Phi|) = m^2 |\Phi|^2, \quad (1.4)$$

where  $m$  is the mass of the scalar field. Part of the aim of such work is to introduce tests to evaluate the reliability of GRHD codes in boson star spacetimes.

They start by considering spherical accretion onto boson stars, the analogue of Bondi-Michel accretion onto BHs [20, 98], which is widely used as a test for GRHD codes. These simulations are one-dimensional, in spherical symmetry, and exclude the origin, placing the inner boundary at  $r = 1.8 M$  or  $r = 3.1 M$ , where from now on  $M$  is the ADM-mass of the boson star. This avoids the fluid shocking with itself and accumulating at the center of the boson star, preserving the stationary character of the Bondi-Michel solution. The authors show that at small distances from the center of the boson star, the behavior of matter differs considerably from the case of BHs.

The second test they present is a stationary torus in hydrodynamic equilibrium around an axially symmetric boson star ( $k = 1$ ,  $\omega = 0.81 m/\hbar$ ). The torus has constant specific angular momentum  $\ell = 4.206$  and is constructed in the way of [1]. The code evolves this stationary solution up to  $t = 10^3 M$  showing still an excellent agreement with the initial condition.

Finally, they consider a non-spherical accretion scenario, where matter is injected in a  $20^\circ$  wedge around the equatorial plane. This wedge is initially a Bondi-Michel flow truncated at  $r = 2 M$ . The boson star used for this simulation is spherically symmetric ( $k = 0$ ,  $\omega = 0.771 m/\hbar$ ), and the simulation is performed in axisymmetry (2.5D). As the system evolves, at first the inflow is decelerated by the increasing thermal pressure. Soon, the the flow reaches the center of the boson star and pro-

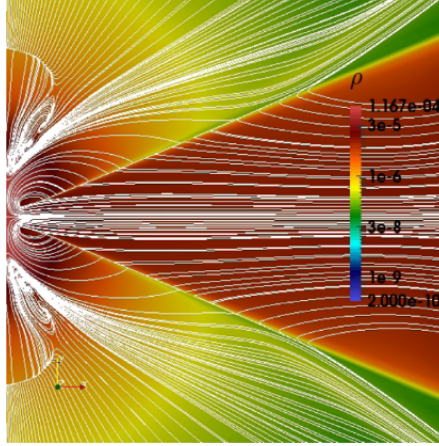


Fig. 1.2: Accretion-ejection region near the center of the boson star in the last simulation by [97]. The color represents logarithmic density, and the white curves are velocity streamlines. From [97].

duces a shock that propagates outwards until it is halted by the supersonic inflow. Later, a spherical structure sustained by pressure gradients appear and propagates out of the boson star. The only direction in which matter can escape is along the poles. Figure 1.2 shows the accretion-ejection region near the center of the boson star. Part of the flow is redirected toward the accretion flow, while another fraction escapes as a thermal wind. The strong radial pressure gradient causes radial of the acceleration of the outflow, which becomes supersonic for  $r > 4 M$ . Finally, interactions between inflow and outflow render the structure unstable, and the shock front changes shape from spherical to triangular. At later stages, the system reaches a quasi-steady state with some variability in the wind intensity. The authors mention that this model does not indicate the presence of Type I (i.e. thermonuclear) X-ray bursts, which are expected to be produced in some models of accretion onto ECOs, and whose absence is considered to strengthen the case of BH candidates in X-ray binaries as true BHs [146]. Overall, this simulation presents a scenario with a phenomenology that is radically different from the case of accretion onto BHs, and invites to consider more diverse scenarios for accretion-ejection flows in compact objects.

#### 1.4.1.2 Tidal disruption of clouds by boson stars

GRHD simulations have also been employed to study the tidal disruption of gas clouds by boson stars. These studies were in part motivated by the pericenter passage in 2014 of the object G2, likely a dusty, ionized gas cloud, in its eccentric orbit around Sgr A\*[60]. simulations of this event were performed by [8] and [125],

among others. However, for horizonless and surfaceless compact objects such as boson stars, tidal disruption would produce a qualitatively different behavior as for BHs. For example, boson stars allow closed orbits with very low angular momentum (including zero). In contrast, for BHs, a cloud approaching with an angular momentum below some threshold would lose a large fraction of its matter behind the event horizon. In addition, matter that falls inside a boson star can in principle form structures inside and continue to emit electromagnetic radiation that may reach a distant observer.

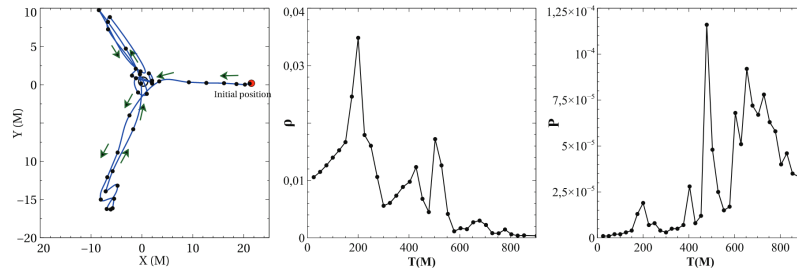


Fig. 1.3: *Left panel:* Trajectory of the center of mass of a cloud initialized at  $23 M$  away from a boson star with  $k = 1$  and  $\omega = 0.8 \text{ m}/\hbar$ . *Center and right panels:* Evolution of the density and pressure maxima for the same simulation, showing spikes that can be associated to flares. From [96].

The first GRHD simulations tidal disruption of clouds by boson stars appeared in [96], also using the code GR-AMRVAC. They consider three cases of falling clouds and two cases of boson stars. Both of the boson stars are made from a free field and are rotating ( $k = 1$ ,  $\omega = 0.8 \text{ m}/\hbar$  and  $k = 4$ ,  $\omega = 0.8 \text{ m}/\hbar$ ). The gas cloud is initialized at rest at different distances from the boson star (23 and 3  $M$ ). It has a Gaussian density profile and is in pressure equilibrium with the ambient medium. Self-gravity is ignored, which is a reasonable approximation, as the gravitational force of the compact object is expected to be much larger due to its proximity. Simulations were two-dimensional and performed in Cartesian quasi-isotropic coordinates on the equatorial plane of the boson stars. This choice avoids spurious effects due to the singularity of the origin of spherical coordinates.

The trajectory of the center of mass of the clouds approximately follows a geodesic. However, close to the boson star, pressure gradients caused by deformations and heating of the cloud produce significant deviations from geodesic motion. At this stage, the cloud acquires a complex structure, which can include shocks propagating against the rotation of the star.

For the case of one of the clouds initialized at a large distance, the combination of tidal stretching, frame dragging and deviations produced by hydrodynamic effects cause the center of mass of the cloud to scatter in the *opposite* direction with respect to the star rotation. In general, the trajectories of the clouds are petal-shaped, with

those initialized at large distance showing more elongated petals (left panel of Figure 1.3).

Following close encounters between the cloud and the boson star, a fraction of the gas is teared off from the cloud by tidal forces. The simulations by [96] show that most of this gas is recaptured by the boson star and forms a disk at its interior, between the last stable orbit and the center of the scalar field torus.

As it could be expected, the passage through the boson star is more violent for the clouds that are initialized at a larger distance. For those cases, the evolution of the pressure and density maximum exhibit several spikes that could be observed as flares (center and right panels of Figure 1.3). The time between flares  $\Delta T$  decreases significantly following the decreasing orbit size of the cloud ( $\Delta T \sim 150, 250, 100, 60 M$ ). In contrast, the cloud that is initialized close to the boson star requires many passages to turn the gas expelled from the cloud into a disk. The spikes in this case appear in larger number and at a more regular separation in time ( $\Delta T \sim 50M$ ). In fact, the orbit of the center of mass is almost completely well described by an ellipse affected by strong precession with an important contribution from frame dragging. The authors suggest that this simulation can be used to study the dynamics of a hot spot orbiting a compact object.

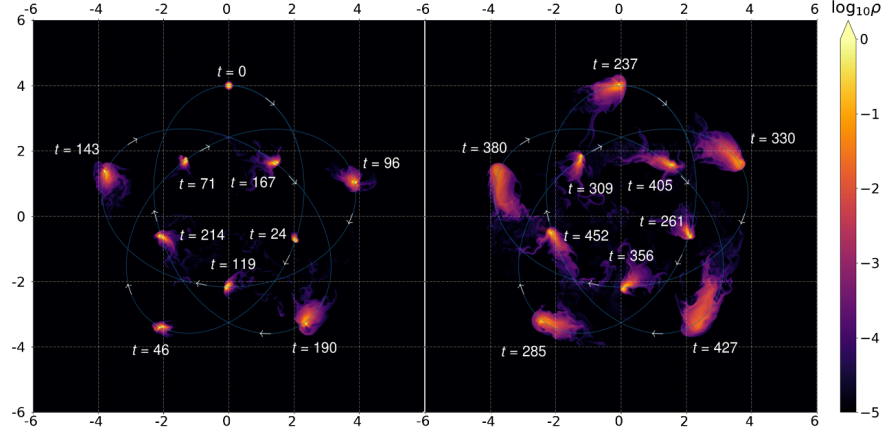


Fig. 1.4: Composite image of a gas cloud closely following a five-petals geodesic around a solitonic star. The cloud experiences several compression-expansion cycles. From [136].

Further simulations of tidal disruption by boson stars were presented by [136]. In such work, the authors perform several simulations for the same boson star model. This is no longer a mini-boson star, but a solitonic boson star, subject to a sextic self-interaction potential

$$U(|\Phi|) = |\Phi|^2(m^2 + a|\Phi|^2 + b|\Phi|^4). \quad (1.5)$$

The parameters chosen for the scalar field are  $m = 1$ ,  $a = -2$ , and  $b = 1$ . The boson star considered has a frequency  $\omega = 0.27 m/\hbar$  and is nonrotating. This object possess a compactness<sup>1</sup>  $\mathcal{C} = 0.4$ , very close to the value  $\mathcal{C} = 0.5$  characteristic of BHs. The boson star considered in this work is nonrotating. These simulations use the GRMHD code BHAC [114, 108] and similarly to those of [97, 96] are performed in a Cartesian coordinate systems. Also in this case, the cloud is not magnetized.

The authors explore four different scenarios for the encounter between a spherical cloud and the boson star, namely, a zero angular momentum orbit, an elliptic orbit, and two circular orbits for different sizes and initial positions of the cloud. For the first three simulations, the cloud is very compact, with a size of  $0.03 M$ . Its initial position is at  $r = 4 M$ , that is, comparable with one initialized at  $r = 3 M$  by [96]. However, the observed behavior differs in important ways from that reported there. This is due to the fact that the boson star is more compact and no longer rotating.

For the the zero-angular momentum case, the motion is now dominated by local tidal forces, instead of the effect of frame dragging. This results in a much faster deformation of the cloud than for the rotating case, due to effects such as compression/expansion cycles and collisions between the cloud and its tail or other debris. For this reason, the cloud survives for a longer time for the case of the elliptic orbit, and even longer for the case of a circular orbit, where interactions between the cloud and its tail are more difficult.

Similarly to the  $r = 3 M$  case reported by [96], the motion of the center of mass for the case with an elliptic orbit can be well described by a geodesic. This is still a precessing ellipse (Figure 1.4), although frame dragging does not contribute to this precession.

For the last boson star-cloud simulation, they place the cloud at a larger distance of  $r = 10 M$  and use a more extended cloud of size  $0.3 M$ . The initial velocity of the cloud is that corresponding to a local circular geodesic. They complement this simulation setup with an identical one where the boson star is replaced by a Schwarzschild BH in order to perform a comparison. For this test, they calculate relevant diagnostics such as the mass accretion rate, a proxy from Bremsstrahlung luminosity to produce a synthetic lightcurve, and a shock detector.

They report that after the tearing of the cloud by tidal forces, the debris starts to accumulate and form a ringlike structure around the boson star. The structure also exhibits an extended spiral shock. The persistence of this structure is in stark contrast with the BH case, where matter disappears behind the horizon, and could result in observable differences. In fact, the synthetic lightcurve produced by the authors not only raises orders of magnitude above that of the BH simulation, but also persists with a nearly constant luminosity for the rest of the simulation at  $t = 1000 M$ . In contrast the lightcurve for the BH case drops to zero once the entire cloud disappears behind the horizon, at  $t = 500 M$ .

---

<sup>1</sup> The compactness of an object is defined as  $\mathcal{C} = R/M$ , where  $R$  is the radius of the object and  $M$  is its mass. Since bosonic stars are extended objects with no clear surface, the authors of [136] define  $R$  as the average radial coordinate weighted by the number density of the bosonic particles.

### 1.4.1.3 Magnetized accretion onto boson stars

Another set of observations that motivated studies on accretion onto boson stars were the very long baseline interferometry (VLBI) campaigns to observe Sgr A\* and M 87\* by the Event Horizon Telescope (EHT) Collaboration. There were great expectations towards the first images of SMBH candidates at a resolution comparable to the angular size of the BHs shadows, and naturally towards the possibility of testing their BH nature (see e.g. Ref. [139]).

To aid with the interpretation of observations, the EHT Collaboration created a library of GRMHD simulations of Kerr BHs with several spins and accreting in different modes (standard and normal evolution (SANE) and magnetically arrested disk (MAD)). These were later postprocessed by general relativistic radiative transfer (GRRT) codes to produce another library, this time of synthetic images and spectra, that could be compared with the real data [2, 33].

In this context, the work of [109] applied the same pipeline to study the observational properties of a boson star in the same accretion regime as the EHT targets, with the goal of assessing the possibility of distinguishing it from a BH by means of the EHT observations. To this end, the authors performed simulations of magnetized accretion onto two members of the family of nonrotating mini boson stars, namely  $\omega M = 0.32$  (hereafter ‘model A’) and  $\omega M = 0.54$  (hereafter ‘model B’). Model A belongs to the unstable branch of the mini boson star family; however, the choice of these models was not based on their stability properties, but with the purpose of exploring two qualitatively different behaviors that can take place also in more general surfaceless and horizonless compact objects, and that may play an important role in their observational properties, as we will discuss later.

The GRMHD simulation setup was similar to that used for the simulations in the EHT library. That is, a torus in hydrodynamic equilibrium around a BH was seeded with a poloidal magnetic field loop, and was slightly perturbed by white noise added to the pressure. This triggered the MRI, which amplified the magnetic field, and started transporting angular momentum outwards, causing the torus material to accrete onto the central object. Due to the prescription chosen for the magnetic field, the simulations were in the SANE regime, that is, Maxwell stresses played a secondary role, and most of the angular momentum transport was mediated by the MRI.

The first and most important difference between the two boson star models originates precisely at this stage. In order for the MRI to be active, the angular velocity profile of the accretion disk  $\Omega(r) := u^r/u^t$  must decrease with the distance from the center of rotation, that is,  $d\Omega/dr < 0$ , where  $u^\mu$  is the 4-velocity of the fluid elements. As the angular momentum is redistributed by the MRI,  $\Omega(r)$  acquires a profile close to that of circular timelike geodesics  $\Omega_K(r)$ , as it is common for SANE simulations (even though not as close as, for example, in thin disk theory). In the Kerr spacetime,  $d\Omega_K/dr < 0$  for all radii, and the instability is always active. However, while this is also the case for boson star B, for boson star A there is a radius  $r_{\text{turn}} > 0$  such that  $d\Omega_K/dr > 0$  for  $r < r_{\text{turn}}$ . As  $\Omega(r)$  gets closer to  $\Omega_K(r)$ , it acquires a maximum where  $d\Omega(r)/dr \approx 0$ , and the instability is suppressed. With no

other means of efficient angular momentum transport, the accretion flow becomes stalled and forms a torus inside the boson star, with its inner edge close to  $r = r_{\text{turn}}$ . This structure appears to be stable and lasts until the end of the simulation.

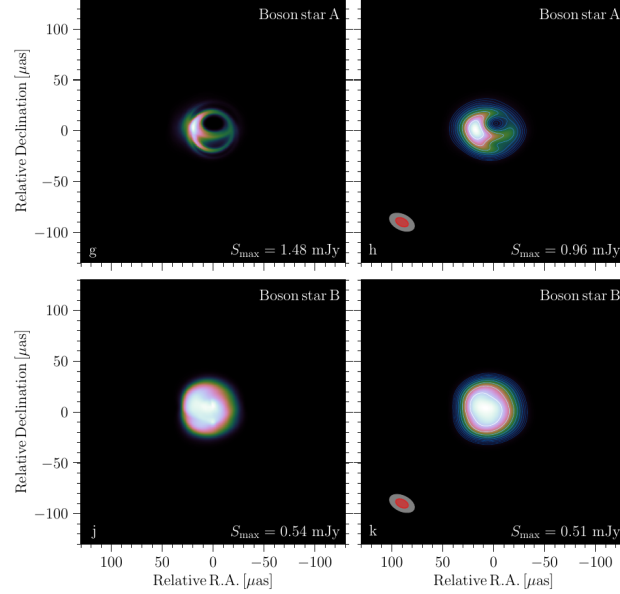


Fig. 1.5: Ray-traced (left column) and synthetic (right column) images at 230 GHz and inclination angle  $60^\circ$  of boson star models A (top row) and B (bottom row). From [109].

When ray-tracing these simulations with the GRRT code `BHOSS` [145, 144], the images produced for each of the boson star models are clearly different (left column of Figure 1.5). Boson star model B has the appearance of a spherical star-like object, while boson star model A exhibits a central brightness depression, resembling the typical image of a BH shadow. This brightness depression corresponds, however, to the evacuated region at the center of the torus enhanced by gravitational lensing. The differences are still clearly noticeable when convolving the GRRT image with 50% of the EHT beam in order to simulate a resolution similar to that achievable by the instrument (right column of Figure 1.5). In particular, the central brightness depression survives.

However, one needs to be cautious before concluding that mini boson stars can mimic supermassive BHs in VLBI observations. One needs to consider, first, that the size of the brightness depression for this boson star is considerably smaller than the one expected for a Kerr BH of the same mass (by 40%), and second that model A belongs to the unstable branch of the family. As the instability can cause the star to collapse to a BH in a timescale of the order of less than an hour for Sgr A\* and less

than a month for M 87\*, this particular model is clearly not viable. It is therefore natural to ask whether there is a member of the family that is stable and at the same time produces a brightness depression of the appropriate size.

This can be estimated by calculating the radius  $r_{\text{turn}}$  and the size of the depression after the enhancement by lensing,  $b(r_{\text{turn}})$ , both of which depend only on the metric and are easy to compute in spherical symmetry, even when the metric is numerical. The results for several members of the mini boson star family are presented in Figure 1.6. It can be seen that no members of the family produce brightness depression with the required size to be mistaken by Kerr BHs given the EHT resolution (of the order of 10  $\mu\text{as}$ ), and that these are all produced on the unstable branch. This numerical experiment therefore rules out mini boson stars as viable models for Sgr A\* and M 87\* under the accretion scenario considered by [109] and under the assumption that  $\Omega(r) \approx \Omega_K(r)$ .

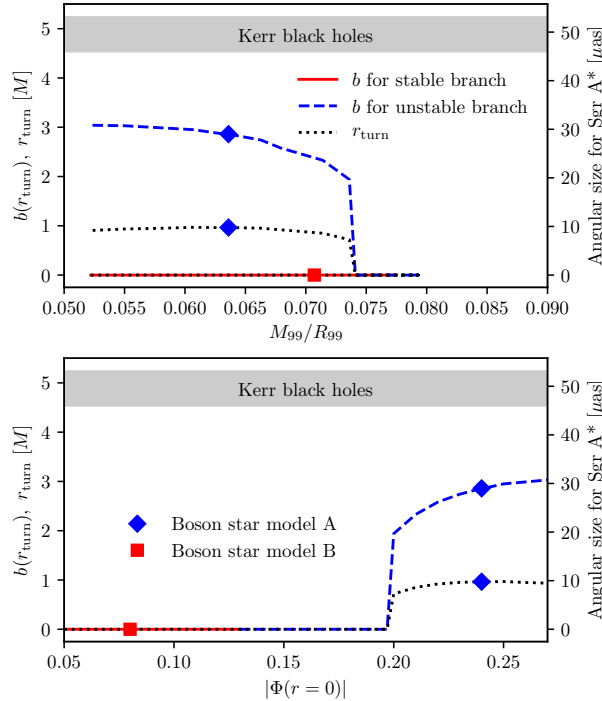


Fig. 1.6: Radial position  $r_{\text{turn}}$  at which the MRI is suppressed and apparent size of the central brightness depression after lensing  $b(r_{\text{turn}})$  for the family of mini-boson stars parametrized by compactness (top panel) and central amplitude of the scalar field (bottom panel). The expected sizes of Kerr BH shadows of the same mass are shown as a shaded region for comparison. From [109].

It is important to remark that this result does not rule out boson stars in general, and consequently neither other horizonless compact objects, as viable models to SMBH candidates. Rather presents a scenario where they could act as BH mimickers by a previously unknown mechanism. In fact, it has been shown that other horizonless compact objects, namely Proca stars, could in principle produce brightness depressions comparable to those of Kerr BHs by this mechanism [71]. On the other hand, it is conceivable that other kinds of ECOs produce central brightness depressions by different mechanisms, such as the nonexistence of timelike circular geodesics below some finite radius, a property present in some rotating boson and Proca stars [130].

It is also important to remark that, there are important differences that may help distinguishing it from a BH shadow. Most importantly, it would not be achromatic phenomenon as it is the case for the latter. For example, its size may vary with the observing frequency, as it is dependent on the optical depth of the fluid. Although at present the images released by the EHT Collaboration are at the single frequency of 230 GHz, there are plans to provide the instrument with multi-frequency capabilities. This would enable us to test the achromaticity of the BH shadow and potentially rule out scenarios as the one presented here.

Besides this, [109] report other differences in simulations of magnetized accretion onto boson stars with respect to what is observed in BH simulations, such as the absence of a jet, which can be explained in part by the lack of rotation, and therefore of the absence of the Blandford-Znajek mechanism; and the presence of quasi-periodic oscillations in the lightcurve of model B, which correspond to the motion of the plasma density maximum around the center of the boson star.

Before concluding this section, it is worth mentioning that the results presented in [109] have the limitation that they only consider the SANE accretion scenario. However, increasing evidence favors instead the MAD scenario for both Sgr A\* and M87\* [2, 33]. It is uncertain whether the formation of the central toroidal structure would also occur for the latter, due to the larger deviations from geodesic motion, the secondary role played by the MRI in angular momentum transport, and the dynamical importance of coherent magnetic fields, which may introduce new unexpected effects. This, however, highlights the importance of performing GRMHD for different models of ECOs under a variety of accretion scenarios.

#### 1.4.1.4 Spherical accretion onto naked singularities

In Reference [16], the authors performed GRHD simulations of quasi-spherical accretion onto a spacetime that contains a naked singularity, namely Kerr spacetimes with dimensionless spin parameter  $a \geq 1$ , also known as *superspinars* [63].

Their simulations adopt as initial and boundary condition a fluid with constant density and pressure, and excise the singularity from the domain by placing an outflow boundary condition at  $r = 0.5 M$  in Boyer-Lindquist coordinates. This is justified by assuming that the singularity is a pathology of GR that should be replaced by something else in the correct underlying theory, but that the detailed descrip-

tion of its unknown properties will not affect significantly the simulation results. Simulations are 2.5D and are performed using the code PLUTO [99].

The authors found accretion patterns that differ qualitatively from the analogous case for BHs, namely Bondi-Michel accretion. The properties of these accretion patterns appear to depend on spin. Below a critical value of  $a \approx 1.4$ , matter is unable to reach the central object due to short-distance repulsion, and instead forms a cloud that continues growing without reaching stationarity. In contrast, simulations above that critical value reach a stationary state in which the central object accretes through a thin equatorial stream. The authors discuss some of the astrophysical implications of both scenarios. In particular, a harder and more intense radiation than for the case of accreting BHs is expected, which they link to the abundance of  $\gamma$ -rays observed in some blazars. They also discuss the possibility of violent events resulting from the collapse of the accreting system onto a black hole.

#### 1.4.1.5 Magnetized accretion onto traversable wormholes

Another interesting example of accretion onto an horizonless, regular, exotic compact object is presented in Reference [34]. In that work, the authors simulate magnetized accretion onto traversable wormholes. Specifically, the spacetimes they consider are described by the Simpson-Visser metric, a two-way traversable wormhole with no rotation. This solution is similar to Schwarzschild from the outside, however it is not in vacuum and requires exotic matter to be sustained. To perform the simulation, the authors assume that this exotic field does not interact with the accreting plasma, and that the latter does not back-react on the field. The simulation set-up is similar to the one described for the boson star case in Section 1.4.1.3 and in typical BH-torus simulations with MRI-driven accretion. However, the disk is initialized only at one side of the wormhole.

The authors employ the code Harm3D and spherical Boyer-Lindquist type coordinates. More specifically, the wormhole metric is given by

$$ds^2 = -f(r)dt^2 + f(r)^{-1}dr^2 + (r^2 + \ell^2)d\Omega^2 \quad (1.6)$$

where  $r(r) := (1 - 2M/\sqrt{r^2 + \ell^2})$  and, in contrast to typical spherical coordinates,  $r \in (-\infty, +\infty)$ . The use of these coordinates allows to cover the whole spacetime with a single chart, with the wormhole throat located at  $r = 0$ . In order to benefit from the properties of radially logarithmic grids, the radial coordinate above is mapped to a numerical coordinate  $x$ , such that  $r = c_r \sinh(x/c_r)$ .

The authors find that, after accretion starts, a portion of the plasma settles at the throat, and forms a rotating cloud roughly  $10^4$  times denser than the accretion disk. This cloud is hot and larger than the light ring, with its emission peaking on the far UV-X-rays for stellar-mass systems. Although no GRRT calculations were performed, this would likely result in the absence of a central brightness depression that could mimic a BH shadow.

The system does not reach equilibrium. Instead, the cloud grows linearly with time, which could result in gravitational collapse onto a BH in less than a Hubble time (also of stellar-mass systems).

Another interesting finding in Reference [34] is that matter falling into the wormhole powers a mildly relativistic thermal wind at the other side of the throat. The efficiency of this outflow (the energy output divided by mass accretion rate) appears to depend on the size of the throat, and for  $\ell = 2.1 M$ , this efficiency is of  $\sim 20\%$ . Astronomical observations from this other side of the wormhole would show a BH-like system that exhibits outflows without an associated inflow, contradicting the typical phenomenology expected for BHs. All of the effects described so far are consequences of the fact that the throat is a minimum of the gravitational potential. This feature is shared by most traversable wormholes, which indicates that these results could apply to many other configurations.

The presence of the central cloud and possible absence of a central brightness depression contradicts some previous expectations on wormhole images, which highlights the importance of performing GRMHD simulations in these spacetimes. Other interesting question that could be answered by future simulations are the effects of spacetime rotation and different initial conditions for the accretion flow.

### 1.4.2 Non-Kerr black holes

As noted above, the Kerr metric [86] can be used to describe stationary and axisymmetric vacuum BH spacetimes. It is obtained as a solution of the dynamical equations of GR and also in several other alternative classical gravity theories, e.g., those that admit GR as a smooth limit.

Non-Kerr BHs have broadly been considered in two contexts. First, allowing for the presence of self-gravitating matter and solving for the appropriate gravitational as well as matter field equations yields a variety of non-Kerr metrics. Examples in GR of such *solution metrics* include (a) the Reissner-Nordström (RN) spacetime (see, e.g., [100]), which contains a static electromagnetic (EM) field, (b) the Kerr-Newman (KN) spacetime [106], which contains a stationary EM field, (c) the Hayward spacetime [67], which contains a static anisotropic fluid (with no viscosity or heat fluxes), (d) the Gibbons-Maeda-Garfinkle-Horowitz-Strominger (GMGHS); [59, 57] spacetime, which contains a dilaton scalar field as well as an EM field, and (e) the Kerr-Sen (KS) spacetime [129], which contains a dilaton, an EM, and an axion field. The nonspinning RN BH and its spinning generalization, the KN BH, both admit two horizons and also possess curvature singularities at  $r = 0$  (in appropriate coordinates). The Hayward BH also admits two horizons but is regular at the center,  $r = 0$ . The GMGHS BH has a single horizon and the same surface gravity as a Schwarzschild BH, independent of the strength of its field content. Together with the KS BH, its spinning counterpart, these arise as solutions to the low-energy effective limit of the heterotic string theory. Examples of non-Kerr BHs in alternative theories include the aforementioned Einstein-scalar-Gauss-Bonnet BHs.

Perhaps the key ambition behind ascertaining whether or not non-Kerr BH solutions can be distinguished from Kerr BHs is to probe both the various types of BH models as well as their underlying theories of gravity and fields for consistency with observations performed on horizon scales.

The second context that has generated interest in the study of non-Kerr BH spacetimes is the attempt to gather further observational evidence for the Kerr hypothesis. This is achieved by working with *parametrized metrics*, which agnostically deform away from the Kerr metric smoothly, making no reference to the field equations. Several parametrized metrics have been designed to capture qualitatively different aspects of possible metric deviations, e.g., the Johannsen-Psaltis (JP) metric [80, 77], the modified gravity bumpy Kerr metric [137, 54], Konoplya-Rezzolla-Zhidenko metric [90], etc.

The Event Horizon Telescope (EHT) observations of M87\* and Sgr A\* [3, 5] are particularly suited to such “tests” of the space of stationary non-Kerr metrics [79, 101, 4, 115, 89, 6]. Since the two EHT sources are supermassive ultracompact objects that are accreting at extremely low rates ( $\sim 10^{-3} M_{\odot} \text{yr}^{-1}$  and  $\lesssim 10^{-7} M_{\odot} \text{yr}^{-1}$  respectively; [3, 5]), their spacetimes are stationary to a very good approximation.

#### 1.4.2.1 Hairy black hole moving through an uniform medium

As mentioned previously, an important motivation to explore the consequences of the existence of ultralight bosonic fields comes from dark matter. To understand the effects of the scalar field in a very general situation, the authors of [38] simulated the flow pattern around a BH with synchronized scalar hair, from now on hairy black hole (HBH), moving through a uniform medium. For a star or a BH, this scenario is known as Bondi-Hoyle-Lyttleton (BHL) accretion [75, 21]. BHL accretion onto a BH is relevant to model several situations of interest to Astronomy, such as a wandering BH moving through the interstellar medium, a BH accreting low angular momentum winds from a binary companion, or a BH in the so called common envelop phase of binary evolution.

The HBH model employed is that from [72], where the scalar field is subject to a quadratic potential (equation 1.4). As it is customary, simulations are performed in the rest frame of the BH. In this frame, the fluid is moving at Mach number  $\mathcal{M} = v_{\infty}/c_{s,\infty} = 5$ , where  $v_{\infty}$  and  $c_{s,\infty}$  are the asymptotic fluid velocity and sound speed, respectively. Four simulations are performed, characterized by different ratios between the mass of the scalar cloud and the ADM mass ( $p := M_{\Phi}/M_{\text{ADM}}$ ), and between the angular momentum of the scalar cloud and the total ADM angular momentum ( $q := J_{\Phi}/J_{\text{ADM}}$ ). The specific values for all simulations were:  $p = (0.53, 0.749, 0.909, 0.982)$  and  $q = (0.128, 0.846, 0.997, 0.998)$ , in the same order.. The simulations are carried out in pure GRHD and in two dimensions on the equatorial plane of the BHs. They employ spherical coordinates and are performed using the code BHAC.

The simulations reveal a flow pattern that is qualitatively similar to that of BHs in BHL accretion, characterized by an upstream bow shock and downstream shock cone. However, the quantitative properties such as the opening angle of the shocks, the location of the stagnation points in units of the BH radius, and the mass accretion rate, depend strongly on the relative importance of the scalar field over the central BH. The authors fit analytical expressions for the mass accretion rate to the numerical results. These could be used to study BH formation and growth scenarios in the presence of ultralight scalar fields.

Similarly to the case of BHL accretion onto BHs [51], the authors observe quasi-periodic oscillations (QPOs) as a result of pressure modes trapped inside the shock cone. The authors study these oscillations by placing detectors close to the stagnation point and producing time series of rest-mass density. They calculate power spectral densities from these time series, and study the effect of the presence of the scalar cloud. Finally, they speculate about the possibility of linking these QPOs with those observed in the X-ray lightcurves of Sgr A\* and some microquasars, and compare them with the observational data.

#### 1.4.2.2 Thin disk accretion onto non-Kerr parameterized black hole

The work of [104] performs GRMHD simulations of accretion onto non-Kerr BHs. However, the spacetimes considered do not belong to any particular theory or model. They come instead from the theory agnostic parameterization known as the Johannsen metric [78]. In this parameterization, four radial functions quantify deviations from the Kerr metric, which are written as series in powers of  $M/r$ . The parameterized metric retains the separability of the Kerr metric that leads to the Carter constant.

Theory-agnostic approaches have the advantage that the metric can be easily written in a convenient form, and can provide a handle on the effect of deviations from the Kerr metric in tests where it is taken as the null hypothesis. The motivation for [104] comes precisely from the possibility of testing the Kerr hypothesis for stellar mass BHs and SMBHs using X-ray spectroscopy and breaking degeneracies in the ISCO size between the BH spin and deviations from Kerr geometry.

For the GRMHD simulations, the authors employ a horizon-penetrating version of the Johannsen metric. They also keep only the leading terms of the expansion of the deviation functions, which results in four deviation parameters. Simulations are performed using the code HARMP I [132], which is based on the HARM family [55]. The authors report seven simulations, most of which are performed in 2.5 dimensions on the meridional plane. Only one simulation is performed in three dimensions as a check for the validity of the two-dimensional results. The initial conditions for the simulations are the similar to those described in Section 1.4.1.3. However, since X-ray reflection spectroscopy is mainly focused on thin accretion disks, a cooling function is added in order to keep the disk thin (with aspect ratio  $H/R = 0.12$ ). Several of the spacetime metrics used share the same value of the ISCO, even when

they have different non-Kerr parameteres switched on and off, and some of them are purely Kerr cases.

The simulation results show that the accretion pattern is similar to that seen in typical GRMHD simulations in the Kerr spacetime. The authors also conclude that semianalytic thin disk models for reflection spectra are a reasonable approximation to their simulations. Finally, they show that even though the total flux can be similar between Kerr and non-Kerr cases, iron line plots are visible different, strengthening the case for X-ray spectroscopy as a sensitive test for deviations with respect to Kerr metric.

To finalize this Section, we would like to remark the usefulness of theory-agnostic parameterized metrics for parameter space surveys that may allow to constrain theories of gravity. Even though currently it is impractical to perform such surveys on GRMHD simulations, due to their high computational cost, understanding the effect of changing the parameters on GRMHD simulations can be used to inform semi-analytic models (such as thin disks) for which surveying the parameter space can be made in a much more efficient way.

#### 1.4.2.3 Magnetized accretion onto dilaton-axion BHs: approaching naked singularities

As noted in Section 1.4.1.3, the EHT observations have been used to produce images of its two main targets, which have been compared against synthetic images produced from state-of-the-art numerical simulations. While such simulations have mostly been performed using the Kerr metric, the first simulations of non-Kerr spacetimes were reported in Ref. [101].

The goal of such work was to assess the capabilities of the EHT array to distinguish between different theories of gravity by observing the BH shadows. To this end, three different simulations of spherically symmetric non-Kerr solutions were performed. These were later postprocessed via GRRT calculations to produce images, which where compared to a simulated image of a Kerr BH (see Figure 1.7). These solutions came from the Einstein-Maxwell-Axion-Dilaton theory [56], which introduces two hypothetical scalar fields (the axion and the dilaton). The three cases considered were selected by matching one of the relevant radii to the value of a Kerr BH, namely, the innermost stable circular orbit (ISCO), the photon ring or the event horizon.

Fig. 1.7, taken from there, shows ray-traced and synthetic time-averaged images (for the Sgr A\*parameters) of a Kerr BH (top row) and a (non-rotating) GMGHS or “dilaton” BH (bottom row), matched to the ISCO. The right column shows synthetic images taking into account the finite resolution of the EHT array, and demonstrates the difficulty in distinguishing the two BHs from a direct comparison of their images. The inclusion of uncertainties from the instrument and observing conditions renders the two BHs practically indistinguishable.

As a follow up of the work by [101], [118] produced new simulations in these nonspinning spacetimes. These included the MAD scenario and more sophisticated

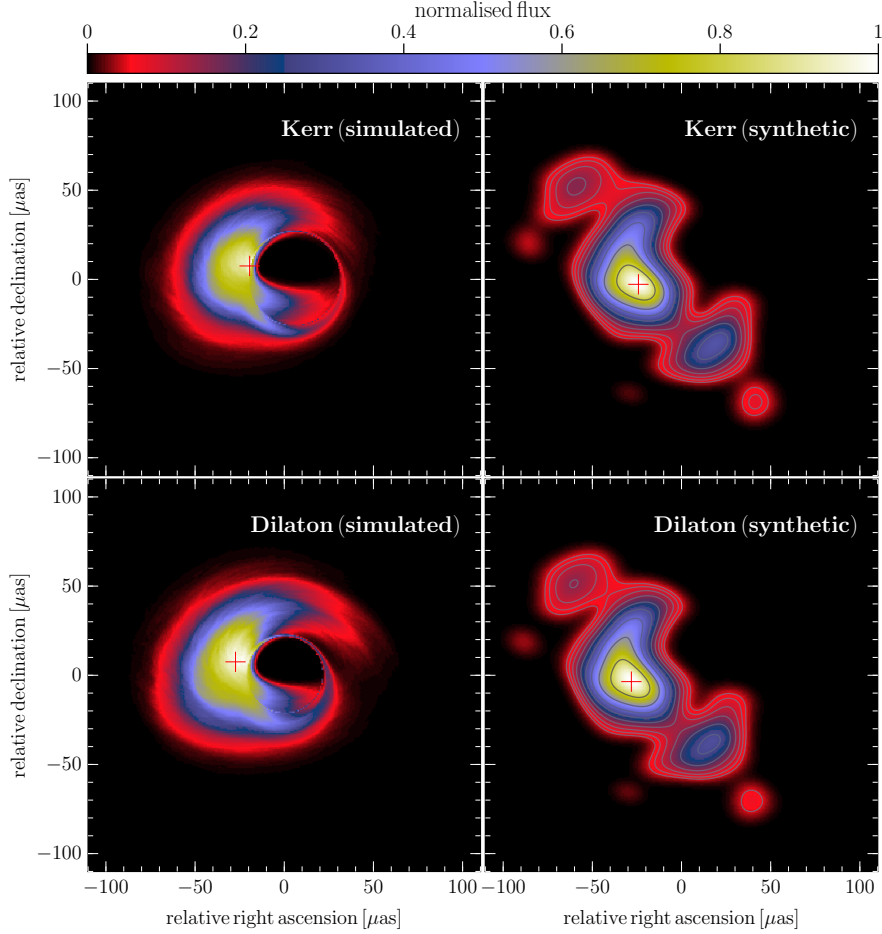


Fig. 1.7: Ray-traced (*left column*) and synthetic (*right columns*) images of a Kerr (*top row*) and a dilaton (*bottom row*) BH simulated in [101]. The two BHs are matched by the ISCO. Credit image: Christian Fromm, Yosuke Mizuno, Ziri Younsi.

radiation models. Some interesting results included a wider jet opening angle and a higher magnetization in the case of the Kerr spacetime.

However, it was also observed that the emission model has a larger effect on the images as compared to the spacetime metric or the accretion model, leading to the conclusion that the imaging approach may not be sufficient to distinguish the two spacetimes with the current resolution of the EHT, as of 2023.

Until recently, accretion in non-Kerr spacetimes has only been explored in non-spinning spacetimes. In Ref. [104], the first 2.5D GRMHD simulation in a spinning non-Kerr spacetime was performed, which we discussed in Sec. 1.4.2.2 above. In Refs. [27, 28], a large number ( $\sim 100$ ) of 3D MAD GRMHD simulations in spin-

ning non-Kerr spacetimes were performed. The first of these studies focussed on accretion onto Kerr-Sen (KS) or “dilaton-axion” BHs, extending the earlier work of Refs. [101, 118] discussed above. The metric for these spacetimes takes the form given in eq. 1.1 above with  $A = r(r + 2D)$  and  $B = r^2 - 2(M - D)r$ .

The right panels of Fig. 1 in Ref. [27] show the time-averaged 230 GHz (the EHT observing frequency) images of four different BHs, two nonspinning and two spinning ones. These are a Schwarzschild BH, a Kerr BH with dimensionless  $a_* = 0.5$ , a near-extremal dilaton BH with dilaton charge  $D = 0.995M$ , and a near-extremal dilaton-axion BH with  $D = 0.5M$  and  $a = 0.49M$ . Since the dilaton spacetime with  $D = 1M$  describes a *naked singularity* spacetime, the dilaton BH image provides hints regarding the image of such *exotic* possibilities.

The M87\* BH parameters are chosen when constructing these images (mass, distance, inclination, etc.). The bright ring in each image is the photon ring [81], a collection of all higher-order images of the entire horizon-scale accretion flow. The photon ring is tightly tied to the BH shadow boundary curve, which is related to its light rings. Observable differences between the sizes of these rings are clear to see in these synthetic images. These differences may be possible to distinguish with future space-based very long baseline interferometry observations, which hope to resolve the photon rings of M87\*.

Similarly, images for three classes of Johannsen-Psaltis parametrized BH spacetimes were constructed in Ref. [28]. The parameters allow one to deform smoothly away from a Kerr geometry, and control qualitatively different aspects of the spacetime. For example, the parameter  $\alpha_{13}$  changes the size of the shadow boundary curve whereas the parameter  $\alpha_{22}$  has a predominant effect on its shape (it changes the BH quadrupole moment) [77]. Thus, measuring the size and shape of the BH shadow from observations can be used to impose constraints on such parameters, and build confidence in the Kerr hypothesis.

#### 1.4.2.4 Energy Extraction from Non-Kerr Black Holes

Thus far we have focussed on the importance of GRMHD simulations in producing realistic synthetic images of accreting BHs, which can directly be compared with the highest angular-resolution images of accreting astrophysical BHs. Such simulations, however, provide yet another rich vein of physical insight: Spinning BHs that accrete magnetized plasma generically produce “jets,” which are relativistic outflows of magnetically-dominated plasmas. Indeed, astrophysical jets are frequently observed across the electromagnetic spectrum (see, e.g., the Hubble Space Telescope image of the M87 jet in Ref. [18]), and much work has been devoted to explaining their production mechanism.

One of the leading proposals is the Blandford-Znajek (BZ) mechanism [19], which is an electromagnetic Penrose process involving spinning BHs [91]. The jet outflow power generated from this mechanism is heuristically understood to be given as  $P \approx a^2 B^2 r_g^2 c$ , where the total energy density in the outflowing plasma is effectively given by the square of the magnetic field strength  $\rho \sim B^2$ , the outflow

speed is  $\approx c$ , the area of cross-section of the outflow is roughly determined by the gravitational radius  $r_g = GM/c^2$ , and the spin of the BH is an important modulating factor. The above can be rewritten as  $P \approx \Phi^2(a/r_g^2)$ , where  $\Phi = Br_g^2$  is the magnetic flux on the horizon, and depends on the specifics of the accretion flow. For Kerr BHs with finite spin, it was shown in Ref. [133] that the remainder  $(a/r_g)^2$  should be replaced by  $\Omega_H^2$ , i.e., the square of the horizon angular velocity, which is determined purely by the spacetime geometry, i.e.,  $P \approx \Phi^2\Omega_H^2$ . The outflow efficiency  $\eta$  defined as  $\eta := P/\dot{M}c^2$  then measures the amount of outflow power per unit of rest mass energy accreted onto the BH. If  $\eta > 1$ , a portion of the outflow energy must be extracted from the “spin energy” of the BH itself, via an (electromagnetic) Penrose process. Assuming the BZ mechanism, the estimate of the jet power has already been used to test the Kerr hypothesis, as proposed in Ref. [14]. For further discussion, we direct the reader to an excellent review of this topic in Ref. [66].

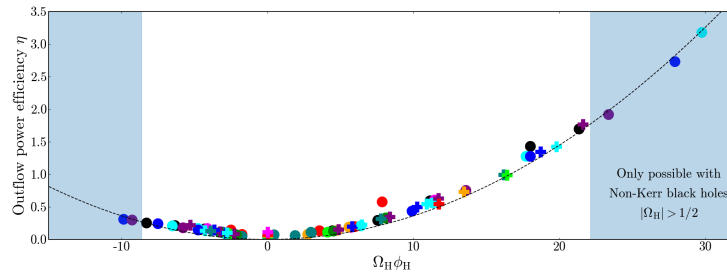


Fig. 1.8: Shown here is the outflow efficiency for Kerr-Sen BHs and Johannsen-Psaltis BHs, and their consistency the BZ prediction. This demonstrates the universality of energy extraction via an electromagnetic Penrose process from various spinning BHs, i.e., Kerr as well as non-Kerr BHs. Adapted from Refs. [27, 28].

Fig. 1.8, taken from Refs. [27, 28], shows the maximum outflow efficiency  $\eta$  computed from MAD GRMHD simulations in  $\sim 100$  different Kerr and non-Kerr BH spacetimes. To compare we also show in the dashed line the analytic prediction  $\eta_{\text{BZ}} \propto (\phi_H \Omega_H)^2$ , where  $\phi_H := \Phi/\sqrt{\dot{M}}$  is the (saturated) dimensionless horizon magnetic flux. This figure demonstrates how the BZ prediction provides an excellent universal description of the jet power in GRMHD simulations. Comparing these universal jet power predictions against actual observations may provide concrete evidence towards establishing the BZ mechanism as the key driver of astrophysical jets in active galactic nuclei. We also note that non-Kerr BHs can produce significantly higher jet powers than Kerr BHs. The application presented in this Section also showcases the insight that can be gained from libraries of simulations, that in this case were generated efficiently by the GPU-accelerated code H-AMR.

Finally, it is worth noting that, assuming the BZ mechanism, estimates of the jet power can be used to test the Kerr hypothesis, as first proposed in Ref. [15].

## 1.5 Future perspectives

In this Chapter, we have presented a landscape of some of the most important families of ECOs, summarized some of the considerations that are in order to performed GRMHD simulations on some of these objects, and have covered the existent literature on the subject while trying to provide the motivation behind each work.

As it can be noticed, the field is extremely young, and there are still many research directions to explore. For instance, regarding horizonless compact objects, it would be interesting to verify via GRMHD simulations whether it is really possible to produce central brightness depressions similar to BH shadows for objects that are dynamically stable, either by the mechanism describe in Section 1.4.1.3, or by different mechanisms. Also, there are currently no simulations of rotating horizonless compact objects, even though such solutions exist. These could be used to study the possible formation of jets, as well as to understand what happens realistically in spacetimes that have peculiar geodesic properties, such as the non-existence of circular timelike orbits. Currently there are also no simulations of ECOs that possess surfaces. A model for the interaction between the surface and the accretion flow could yield new observational signatures to constrain the existence of these objects. A different problem, also related to boundary conditions, is that of the treatment of naked singularities within a fluid simulation. This research line would allow to extend the work on imaging such exotic objects, which so far has considered only ray-traced images with no underlying GRMHD model.

Another natural extension of existing simulations could come from taking into consideration interactions between the additional fundamental fields that are present in many ECO models. In fact, some of these fields (e.g. dilatons and axions) are expected to interact with matter or the electromagnetic field, but these interactions have so far been neglected. Such simulations could help predicting signatures of new fundamental fields even in cases where the latter are not sufficiently strong to produce a significant gravitational interaction.

Finally, another direction that we expect to be very fruitful is the production of libraries of simulated data. Besides allowing us to identify trends as in the works described in Section 1.4.2.4, this would allow to systematically constrain parameters for ECOs based on observations, and ultimately test their existence.

**Acknowledgements** We thank Z. Meliani, M. C. Teodoro, C. Fromm, Y. Mizuno and Z. Younsi for granting permission to reproduce their figures. HO is supported by the Individual CEEC program - 5th edition funded by the Portuguese Foundation for Science and Technology (FCT). This work is supported by the Center for Research and Development in Mathematics and Applications (CIDMA) through the Portuguese Foundation for Science and Technology (FCT - Fundação para a Ciência e a Tecnologia), references UIDB/04106/2020, UIDP/04106/2020 (<https://doi.org/10.54499/UIDB/04106/2020> and <https://doi.org/10.54499/UIDP/04106/2020>). The authors acknowledge support from the projects PTDC/FIS-AST/3041/2020, CERN/FIS-PAR/0024/2021 and 2022.04560.PTDC. This work has further been supported by the European Union’s Horizon 2020 research and innovation (RISE) programme H2020-MSCA-RISE-2017 Grant No. FunFiCO-777740 and by the European Horizon Europe staff exchange (SE) programme HORIZON-MSCA-2021-SE-01 Grant No. NewFunFiCO-10108625.

## References

- [1] Abramowicz, M., Jaroszynski, M., and Sikora, M. (1978). *Relativistic, accreting disks*. A&A, 63:221–224.
- [2] Akiyama, K., Alberdi, A., Alef, W., et al. (2019). *First M87 Event Horizon Telescope Results. V. Physical Origin of the Asymmetric Ring*. The Astrophysical Journal, 875(1):L5. Publisher: IOP Publishing.
- [3] Akiyama, K. et al. (2019). *First M87 Event Horizon Telescope Results. I. The Shadow of the Supermassive Black Hole*. *Astrophys. J. Lett.*, 875:L1.
- [4] Akiyama, K. et al. (2019). *First M87 Event Horizon Telescope Results. VI. The Shadow and Mass of the Central Black Hole*. *Astrophys. J. Lett.*, 875(1):L6.
- [5] Akiyama, K. et al. (2022). *First Sagittarius A\* Event Horizon Telescope Results. I. The Shadow of the Supermassive Black Hole in the Center of the Milky Way*. *ApJL*, 930(2):L12.
- [6] Akiyama, K. et al. (2022). *First Sagittarius A\* Event Horizon Telescope Results. VI. Testing the Black Hole Metric*. *ApJL*, 930(2):L17.
- [7] Almheiri, A., Marolf, D., Polchinski, J., et al. (2013). *Black Holes: Complementarity or Firewalls?* *JHEP*, 02:062.
- [8] Anninos, P., Fragile, P. C., Wilson, J., et al. (2012). *THREE-DIMENSIONAL MOVING-MESH SIMULATIONS OF GALACTIC CENTER CLOUD G2*. *The Astrophysical Journal*, 759(2):132. Publisher: The American Astronomical Society.
- [9] Antoniou, G., Bakopoulos, A., and Kanti, P. (2018). *Evasion of No-Hair Theorems and Novel Black-Hole Solutions in Gauss-Bonnet Theories*. *Phys. Rev. Lett.*, 120(13):131102.
- [10] Arnowitt, R., Deser, S., and Misner, C. W. (2008). *Republication of: The dynamics of general relativity*. *Gen. Rel. Grav.*, 40(9):1997–2027.
- [11] Azreg-Aïnou, M. (2014). *From static to rotating to conformal static solutions: rotating imperfect fluid wormholes with(out) electric or magnetic field*. *Eur. Phys. J. C*, 74:2865.
- [12] Azreg-Aïnou, M. (2014). *Generating rotating regular black hole solutions without complexification*. *Phys. Rev. D*, 90(6):064041.
- [13] Azreg-Aïnou, M. (2014). *Regular and conformal regular cores for static and rotating solutions*. *Phys. Lett. B*, 730:95–98.
- [14] Bambi, C. (2012). *Attempt to find a correlation between the spin of stellar-mass black hole candidates and the power of steady jets: Relaxing the Kerr black hole hypothesis*. *Physical Review D*, 86:123013. Publisher: APS ADS Bibcode: 2012PhRvD..86l3013B.
- [15] Bambi, C. (2012). *Attempt to find a correlation between the spin of stellar-mass black hole candidates and the power of steady jets: Relaxing the Kerr black hole hypothesis*. *Phys. Rev. D*, 86(12):123013.
- [16] Bambi, C., Freese, K., Harada, T., et al. (2009). *Accretion process onto super-spinning objects*. *Physical Review D*, 80(10):104023. Publisher: American Physical Society.

- [17] Berti, E., Collodel, L. G., Kleihaus, B., *et al.* (2021). *Spin-induced black-hole scalarization in Einstein-scalar-Gauss-Bonnet theory*. Phys. Rev. Lett., 126(1):011104.
- [18] Biretta, J. A., Sparks, W. B., and Macchetto, F. (1999). *Hubble Space Telescope Observations of Superluminal Motion in the M87 Jet*. ApJ, 520(2):621–626.
- [19] Blandford, R. D. and Znajek, R. L. (1977). *Electromagnetic extraction of energy from Kerr black holes*. MNRAS, 179:433–456.
- [20] Bondi, H. (1952). *On Spherically Symmetrical Accretion*. Monthly Notices of the Royal Astronomical Society, 112(2):195–204.
- [21] Bondi, H. and Hoyle, F. (1944). *On the mechanism of accretion by stars*. Monthly Notices of the Royal Astronomical Society, 104:273. ADS Bibcode: 1944MNRAS.104..273B.
- [22] Boyer, R. H. and Lindquist, R. W. (1967). *Maximal Analytic Extension of the Kerr Metric*. Journal of Mathematical Physics, 8(2):265–281.
- [23] Brito, R., Cardoso, V., Herdeiro, C. A. R., *et al.* (2016). *Proca stars: Gravitating Bose–Einstein condensates of massive spin 1 particles*. Phys. Lett. B, 752:291–295.
- [24] Brito, R., Cardoso, V., and Pani, P. (2015). *Superradiance: New Frontiers in Black Hole Physics*. Lect. Notes Phys., 906:pp.1–237.
- [25] Cardoso, V., Franzin, E., and Pani, P. (2016). *Is the gravitational-wave ringdown a probe of the event horizon?* Phys. Rev. Lett., 116(17):171101. [Erratum: Phys. Rev. Lett. 117, 089902 (2016)].
- [26] Cardoso, V. and Pani, P. (2019). *Testing the nature of dark compact objects: a status report*. Living Rev. Rel., 22(1):4.
- [27] Chatterjee, K., Kocherlakota, P., Younsi, Z., *et al.* (2023). *Energy Extraction from Spinning Stringy Black Holes*.
- [28] Chatterjee, K., Younsi, Z., Kocherlakota, P., *et al.* (2023). *On the Universality of Energy Extraction from Black Hole Spacetimes*.
- [29] Choquet-Bruhat, Y. and Geroch, R. P. (1969). *Global aspects of the Cauchy problem in general relativity*. Commun. Math. Phys., 14:329–335.
- [30] Clough, K., Helfer, T., Witek, H., *et al.* (2022). *Ghost Instabilities in Self-Interacting Vector Fields: The Problem with Proca Fields*. Phys. Rev. Lett., 129(15):151102.
- [31] Coates, A. and Ramazanoğlu, F. M. (2023). *Coordinate singularities of self-interacting vector field theories*. Phys. Rev. Lett., 130:021401.
- [32] Coates, A. and Ramazanoğlu, F. M. (2022). *Intrinsic Pathology of Self-Interacting Vector Fields*. Phys. Rev. Lett., 129(15):151103.
- [33] Collaboration, E. H. T., Akiyama, K., Alberdi, A., *et al.* (2022). *First Sagittarius A\* Event Horizon Telescope Results. VI. Testing the Black Hole Metric*. The Astrophysical Journal Letters, 930(2):L17. Publisher: The American Astronomical Society.
- [34] Combi, L., Yang, H., Gutierrez, E., *et al.* (2024). *General relativistic magnetohydrodynamical simulations of accretion flows through traversable worm-*

holes. *Physical Review D*, 109(10):103034. Publisher: American Physical Society.

[35] Comins, N. and Schutz, B. F. (1978). *On the Ergoregion Instability*. Proceedings of the Royal Society of London Series A, 364(1717):211–226.

[36] Cruz-Osorio, A., Gimeno-Soler, S., and Font, J. A. (2020). *Non-linear evolutions of magnetized thick discs around black holes: dependence on the initial data*. *Monthly Notices of the Royal Astronomical Society*, 492(4):5730–5742.

[37] Cruz-Osorio, A., Lora-Clavijo, F. D., and Guzmán, F. S. (2012). *Is the flip-flop behaviour of accretion shock cones on to black holes an effect of coordinates?* *Monthly Notices of the Royal Astronomical Society*, 426(1):732–738.

[38] Cruz-Osorio, A., Rezzolla, L., Lora-Clavijo, F. D., *et al.* (2023). *Bondi-Hoyle-Lyttleton accretion onto a rotating black hole with ultralight scalar hair*. *Journal of Cosmology and Astroparticle Physics*, 2023(08):057. Publisher: IOP Publishing.

[39] Cunha, P. V. P., Berti, E., and Herdeiro, C. A. R. (2017). *Light-Ring Stability for Ultracompact Objects*. *Phys. Rev. Lett.*, 119(25):251102.

[40] Cunha, P. V. P., Grover, J., Herdeiro, C., *et al.* (2016). *Chaotic lensing around boson stars and Kerr black holes with scalar hair*. *Phys. Rev. D*, 94(10):104023.

[41] Cunha, P. V. P., Herdeiro, C., Radu, E., *et al.* (2023). *Exotic Compact Objects and the Fate of the Light-Ring Instability*. *Phys. Rev. Lett.*, 130(6):061401.

[42] Cunha, P. V. P. and Herdeiro, C. A. R. (2020). *Stationary black holes and light rings*. *Phys. Rev. Lett.*, 124(18):181101.

[43] Cunha, P. V. P., Herdeiro, C. A. R., Kleihaus, B., *et al.* (2017). *Shadows of Einstein–dilaton–Gauss–Bonnet black holes*. *Phys. Lett. B*, 768:373–379.

[44] Cunha, P. V. P., Herdeiro, C. A. R., and Radu, E. (2017). *Fundamental photon orbits: black hole shadows and spacetime instabilities*. *Phys. Rev. D*, 96(2):024039.

[45] Cunha, P. V. P., Herdeiro, C. A. R., and Radu, E. (2019). *EHT constraint on the ultralight scalar hair of the M87 supermassive black hole*. *Universe*, 5(12):220.

[46] Cunha, P. V. P., Herdeiro, C. A. R., and Radu, E. (2019). *Spontaneously Scalarized Kerr Black Holes in Extended Scalar-Tensor–Gauss–Bonnet Gravity*. *Phys. Rev. Lett.*, 123(1):011101.

[47] Cunha, P. V. P., Herdeiro, C. A. R., Radu, E., *et al.* (2015). *Shadows of Kerr black holes with scalar hair*. *Phys. Rev. Lett.*, 115(21):211102.

[48] Das, P. and Porth, O. (2023). *Three-dimensional GRMHD simulations of neutron star jets*. ArXiv:2311.05301 [astro-ph].

[49] Delgado, J. F. M., Herdeiro, C. A. R., and Radu, E. (2022). *Equatorial timelike circular orbits around generic ultracompact objects*. *Phys. Rev. D*, 105(6):064026.

[50] Doneva, D. D. and Yazadjiev, S. S. (2018). *New Gauss–Bonnet Black Holes with Curvature-Induced Scalarization in Extended Scalar-Tensor Theories*. *Phys. Rev. Lett.*, 120(13):131103.

- [51] Dönmez, O., Zanotti, O., and Rezzolla, L. (2011). *On the development of quasi-periodic oscillations in Bondi–Hoyle accretion flows*. Monthly Notices of the Royal Astronomical Society, 412(3):1659–1668.
- [52] Fernandes, P. G. S., Burrage, C., Eichhorn, A., *et al.* (2024). *Shadows and Properties of Spin-Induced Scalarized Black Holes with and without a Ricci Coupling*.
- [53] Font, J. A., Ibanez, J. M., and Papadopoulos, P. (1998). A 'Horizon adapted' approach to the study of relativistic accretion flows onto rotating black holes. *Astrophys. J. Lett.*, 507:L67.
- [54] Gair, J. and Yunes, N. (2011). Approximate waveforms for extreme-mass-ratio inspirals in modified gravity spacetimes. *Phys. Rev. D*, 84(6):064016.
- [55] Gammie, C. F., McKinney, J. C., and Tóth, G. (2003). *HARM: A Numerical Scheme for General Relativistic Magnetohydrodynamics*. *The Astrophysical Journal*, 589(1):444. Publisher: IOP Publishing.
- [56] García, A., Galtsov, D., and Kechkin, O. (1995). *Class of Stationary Axisymmetric Solutions of the Einstein–Maxwell–Dilaton–Axion Field Equations*. *Physical Review Letters*, 74(8):1276–1279. Publisher: American Physical Society.
- [57] Garfinkle, D., Horowitz, G. T., and Strominger, A. (1991). *Charged black holes in string theory*. *Phys. Rev. D*, 43:3140. [Erratum: *Phys. Rev. D* 45, 3888 (1992)].
- [58] Ghosh, R. and Sarkar, S. (2021). *Light rings of stationary spacetimes*. *Phys. Rev. D*, 104(4):044019.
- [59] Gibbons, G. W. and Maeda, K.-i. (1988). *Black Holes and Membranes in Higher Dimensional Theories with Dilaton Fields*. *Nucl. Phys. B*, 298:741–775.
- [60] Gillessen, S., Genzel, R., Fritz, T. K., *et al.* (2012). *A gas cloud on its way towards the supermassive black hole at the Galactic Centre*. *Nature*, 481(7379):51–54. Publisher: Nature Publishing Group.
- [61] Gimeno-Soler, S., Font, J. A., Herdeiro, C., *et al.* (2019). *Magnetized accretion disks around Kerr black holes with scalar hair: Constant angular momentum disks*. *Phys. Rev. D*, 99(4):043002.
- [62] Gimeno-Soler, S., Font, J. A., Herdeiro, C., *et al.* (2021). *Magnetized accretion disks around Kerr black holes with scalar hair: Nonconstant angular momentum disks*. *Phys. Rev. D*, 104(10):103008.
- [63] Gimon, E. G. and Hořava, P. (2009). *Astrophysical violations of the Kerr bound as a possible signature of string theory*. *Physics Letters B*, 672(3):299–302.
- [64] Grandclément, P. (2010). *KADATH: A spectral solver for theoretical physics*. *Journal of Computational Physics*, 229(9):3334–3357.
- [65] Hawking, S. W. (1976). *Breakdown of Predictability in Gravitational Collapse*. *Phys. Rev. D*, 14:2460–2473.
- [66] Hawley, J. F., Fendt, C., Hardcastle, M., *et al.* (2015). *Disks and Jets. Gravity, Rotation and Magnetic Fields*. *Space Sci. Rev.*, 191(1-4):441–469.

- [67] Hayward, S. A. (2006). *Formation and Evaporation of Nonsingular Black Holes*. Phys. Rev. Lett., 96(3):031103.
- [68] Herdeiro, C., Perapechka, I., Radu, E., *et al.* (2019). *Asymptotically flat spinning scalar, Dirac and Proca stars*. Phys. Lett. B, 797:134845.
- [69] Herdeiro, C., Radu, E., and Rúnarsson, H. (2016). *Kerr black holes with Proca hair*. Class. Quant. Grav., 33(15):154001.
- [70] Herdeiro, C. A. R. (2023). *Black Holes: On the Universality of the Kerr Hypothesis*. Lect. Notes Phys., 1017:315–331.
- [71] Herdeiro, C. A. R., Pombo, A. M., Radu, E., *et al.* (2021). *The imitation game: Proca stars that can mimic the Schwarzschild shadow*. Journal of Cosmology and Astroparticle Physics, 2021(04):051. Publisher: IOP Publishing.
- [72] Herdeiro, C. A. R. and Radu, E. (2014). *Kerr black holes with scalar hair*. Phys. Rev. Lett., 112:221101.
- [73] Herdeiro, C. A. R., Radu, E., Sanchis-Gual, N., *et al.* (2024). *The non-spherical ground state of Proca stars*. Phys. Lett. B, 852:138595.
- [74] Herdeiro, C. A. R., Radu, E., Silva, H. O., *et al.* (2021). *Spin-induced scalarized black holes*. Phys. Rev. Lett., 126(1):011103.
- [75] Hoyle, F. and Lyttleton, R. A. (1939). *The effect of interstellar matter on climatic variation*. Mathematical Proceedings of the Cambridge Philosophical Society, 35(3):405–415.
- [76] Hui, L., Ostriker, J. P., Tremaine, S., *et al.* (2017). *Ultralight scalars as cosmological dark matter*. Phys. Rev. D, 95(4):043541.
- [77] Johannsen, T. (2013). *Regular black hole metric with three constants of motion*. Phys. Rev. D, 88(4):044002.
- [78] Johannsen, T. (2013). *Regular black hole metric with three constants of motion*. Physical Review D, 88(4):044002. Publisher: American Physical Society.
- [79] Johannsen, T. and Psaltis, D. (2010). *Testing the No-Hair Theorem with Observations in the Electromagnetic Spectrum: II. Black-Hole Images*. Astrophy. J., 718:446–454.
- [80] Johannsen, T. and Psaltis, D. (2011). *A Metric for Rapidly Spinning Black Holes Suitable for Strong-Field Tests of the No-Hair Theorem*. Phys. Rev. D, 83:124015.
- [81] Johnson, M. D. *et al.* (2020). *Universal interferometric signatures of a black hole's photon ring*. Sci. Adv., 6(12):eaaz1310.
- [82] Joshi, A. B., Dey, D., Joshi, P. S., *et al.* (2020). *Shadow of a Naked Singularity without Photon Sphere*. Phys. Rev. D, 102(2):024022.
- [83] Kanti, P., Mavromatos, N. E., Rizos, J., *et al.* (1996). *Dilatonic black holes in higher curvature string gravity*. Phys. Rev. D, 54:5049–5058.
- [84] Kaup, D. J. (1968). *Klein-Gordon Geon*. Phys. Rev., 172:1331–1342.
- [85] Keir, J. (2016). *Slowly decaying waves on spherically symmetric spacetimes and ultracompact neutron stars*. Class. Quant. Grav., 33(13):135009.
- [86] Kerr, R. P. (1963). *Gravitational field of a spinning mass as an example of algebraically special metrics*. Phys. Rev. Lett., 11:237–238.

- [87] Kleihaus, B., Kunz, J., and Radu, E. (2011). *Rotating Black Holes in Dilatonic Einstein-Gauss-Bonnet Theory*. Phys. Rev. Lett., 106:151104.
- [88] Kocherlakota, P., Narayan, R., Chatterjee, K., *et al.* (2023). *Toward General Relativistic Magnetohydrodynamics Simulations in Stationary Nonvacuum Spacetimes*. Astrophys. J. Lett., 956(1):L11.
- [89] Kocherlakota, P. *et al.* (2021). *Constraints on black-hole charges with the 2017 EHT observations of M87\**. Phys. Rev. D, 103(10):104047.
- [90] Konoplya, R., Rezzolla, L., and Zhidenko, A. (2016). *General parametrization of axisymmetric black holes in metric theories of gravity*. Phys. Rev. D, 93(6):064015.
- [91] Lasota, J. P., Gourgoulhon, E., Abramowicz, M., *et al.* (2014). *Extracting black-hole rotational energy: The generalized Penrose process*. Phys. Rev. D, 89(2):024041.
- [92] Liebling, S. L. and Palenzuela, C. (2023). *Dynamical boson stars*. Living Rev. Rel., 26(1):1.
- [93] Mathur, S. D. (2008). *Fuzzballs and the information paradox: A Summary and conjectures*.
- [94] Mazur, P. O. and Mottola, E. (2004). *Gravitational vacuum condensate stars*. Proc. Nat. Acad. Sci., 101:9545–9550.
- [95] McKinney, J. C. and Gammie, C. F. (2004). *A Measurement of the electromagnetic luminosity of a Kerr black hole*. Astrophys. J., 611:977–995.
- [96] Meliani, Z., Casse, F., Grandclément, P., *et al.* (2017). *On tidal disruption of clouds and disk formation near boson stars*. Classical and Quantum Gravity, 34(22):225003. Publisher: IOP Publishing.
- [97] Meliani, Z., Grandclément, P., Casse, F., *et al.* (2016). *GR-AMRVAC code applications: accretion onto compact objects, boson stars versus black holes*. Classical and Quantum Gravity, 33(15):155010. Publisher: IOP Publishing.
- [98] Michel, F. C. (1972). *Accretion of matter by condensed objects*. Astrophysics and Space Science, 15(1):153–160. Publisher: Kluwer Academic Publishers.
- [99] Mignone, A., Bodo, G., Massaglia, S., *et al.* (2007). *PLUTO: A Numerical Code for Computational Astrophysics*. The Astrophysical Journal Supplement Series, 170:228–242. Publisher: IOP ADS Bibcode: 2007ApJS..170..228M.
- [100] Misner, C. W., Thorne, K. S., and Wheeler, J. A. (1973). *Gravitation*.
- [101] Mizuno, Y., Younsi, Z., Fromm, C. M., *et al.* (2018). *The current ability to test theories of gravity with black hole shadows*. Nature Astronomy, 2(7):585–590. Publisher: Nature Publishing Group.
- [102] Morris, M. S. and Thorne, K. S. (1988). *Wormholes in space-time and their use for interstellar travel: A tool for teaching general relativity*. Am. J. Phys., 56:395–412.
- [103] Mou, Z.-G. and Zhang, H.-Y. (2022). *Singularity Problem for Interacting Massive Vectors*. Phys. Rev. Lett., 129(15):151101.
- [104] Nampalliwar, S., Yfantis, A. I., and Kokkotas, K. D. (2022). *Extending GRMHD for thin disks to non-Kerr spacetimes*. Physical Review D, 106(6):063009. Publisher: American Physical Society.

- [105] Narayan, R. and McClintock, J. E. (2013). *Observational Evidence for Black Holes*. arXiv preprint arXiv:1312.6698, (1944):21. ArXiv: 1312.6698.
- [106] Newman, E. T., Couch, R., Chinnapared, K., *et al.* (1965). *Metric of a Rotating, Charged Mass*. *J. Math. Phys.*, 6:918–919.
- [107] Newman, E. T. and Janis, A. I. (1965). *Note on the Kerr spinning particle metric*. *J. Math. Phys.*, 6:915–917.
- [108] Olivares, H., Porth, O., Davelaar, J., *et al.* (2019). *Constrained transport and adaptive mesh refinement in the Black Hole Accretion Code*. *Astronomy & Astrophysics*, 629:A61. Publisher: EDP Sciences.
- [109] Olivares, H., Younsi, Z., Fromm, C. M., *et al.* (2020). *How to tell an accreting boson star from a black hole*. *Monthly Notices of the Royal Astronomical Society*, 497(1):521–535.
- [110] Ortiz, N., Sarbach, O., and Zannias, T. (2015). *Shadow of a naked singularity*. *Phys. Rev. D*, 92(4):044035.
- [111] Parfrey, K. and Tchekhovskoy, A. (2017). *General-relativistic Simulations of Four States of Accretion onto Millisecond Pulsars*. *The Astrophysical Journal Letters*, 851(2):L34. Publisher: The American Astronomical Society.
- [112] Penrose, R. (1965). *Gravitational collapse and space-time singularities*. *Phys. Rev. Lett.*, 14:57–59.
- [113] Poisson, E. (2004). *A Relativist's Toolkit: The Mathematics of Black-Hole Mechanics*.
- [114] Porth, O., Olivares, H., Mizuno, Y., *et al.* (2017). *The Black Hole Accretion Code*. *Computational Astrophysics and Cosmology*, 4(1):1. ArXiv: 1611.09720 Publisher: Springer International Publishing.
- [115] Psaltis, D. *et al.* (2020). *Gravitational Test Beyond the First Post-Newtonian Order with the Shadow of the M87 Black Hole*. *Phys. Rev. Lett.*, 125(14):141104.
- [116] Regge, T. and Wheeler, J. A. (1957). *Stability of a Schwarzschild singularity*. *Phys. Rev.*, 108:1063–1069.
- [117] Ripley, J. L. and Pretorius, F. (2020). *Scalarized Black Hole dynamics in Einstein dilaton Gauss-Bonnet Gravity*. *Phys. Rev. D*, 101(4):044015.
- [118] Röder, J., Cruz-Osorio, A., Fromm, C. M., *et al.* (2023). *Probing the space-time and accretion model for the Galactic Center: Comparison of Kerr and dilaton black hole shadows*. *Astron. Astrophys.*, 671:A143.
- [119] Rosa, J. a. L., Garcia, P., Vincent, F. H., *et al.* (2022). *Observational signatures of hot spots orbiting horizonless objects*. *Phys. Rev. D*, 106(4):044031.
- [120] Rosa, J. a. L., Macedo, C. F. B., and Rubiera-Garcia, D. (2023). *Imaging compact boson stars with hot spots and thin accretion disks*. *Phys. Rev. D*, 108(4):044021.
- [121] Rosa, J. a. L., Pelle, J., and Pérez, D. (2024). *Accretion disks and relativistic line broadening in boson star spacetimes*.
- [122] Rosa, J. a. L. and Rubiera-Garcia, D. (2022). *Shadows of boson and Proca stars with thin accretion disks*. *Phys. Rev. D*, 106(8):084004.

- [123] Ruffini, R. and Bonazzola, S. (1969). *Systems of selfgravitating particles in general relativity and the concept of an equation of state*. Phys. Rev., 187:1767–1783.
- [124] Sanchis-Gual, N., Di Giovanni, F., Zilhão, M., *et al.* (2019). *Nonlinear Dynamics of Spinning Bosonic Stars: Formation and Stability*. Phys. Rev. Lett., 123(22):221101.
- [125] Schartmann, M., Burkert, A., Alig, C., *et al.* (2012). *SIMULATIONS OF THE ORIGIN AND FATE OF THE GALACTIC CENTER CLOUD G2*. The Astrophysical Journal, 755(2):155. Publisher: The American Astronomical Society.
- [126] Schunck, F. E. and Mielke, E. W. (1998). *Rotating boson star as an effective mass torus in general relativity*. Phys. Lett. A, 249:389–394.
- [127] Schwarzschild, K. (1916). *On the gravitational field of a mass point according to Einstein's theory*. Sitzungsber. Preuss. Akad. Wiss. Berlin (Math. Phys.), 1916:189–196.
- [128] Seidel, E. and Suen, W.-M. (1994). *Formation of solitonic stars through gravitational cooling*. Phys. Rev. Lett., 72:2516–2519.
- [129] Sen, A. (1992). *Rotating charged black hole solution in heterotic string theory*. Phys. Rev. Lett., 69:1006–1009.
- [130] Sengo, I., Cunha, P. V. P., Herdeiro, C. A. R., *et al.* (2024). *The imitation game reloaded: effective shadows of dynamically robust spinning Proca stars*. ArXiv:2402.14919 [astro-ph, physics:gr-qc].
- [131] Silva, H. O., Sakstein, J., Gualtieri, L., *et al.* (2018). *Spontaneous scalarization of black holes and compact stars from a Gauss-Bonnet coupling*. Phys. Rev. Lett., 120(13):131104.
- [132] Tchekhovskoy, A. (2019). *HARMPI*. <https://github.com/atchekho/harmpi.git>.
- [133] Tchekhovskoy, A., Narayan, R., and McKinney, J. C. (2010). *Black Hole Spin and The Radio Loud/Quiet Dichotomy of Active Galactic Nuclei*. ApJ, 711(1):50–63.
- [134] Teodoro, M., Collodel, L., Doneva, D., *et al.* (2021). *Thick toroidal configurations around scalarized Kerr black holes*. Physical Review D, 104(12):124047. Publisher: American Physical Society.
- [135] Teodoro, M. C., Collodel, L. G., and Kunz, J. (2021). *Retrograde polish doughnuts around boson stars*. Journal of Cosmology and Astroparticle Physics, 2021(03):063. Publisher: IOP Publishing.
- [136] Teodoro, M. C., Collodel, L. G., and Kunz, J. (2021). *Tidal effects in the motion of gas clouds around boson stars*. Physical Review D, 103(10):104064. Publisher: American Physical Society.
- [137] Vigeland, S., Yunes, N., and Stein, L. (2011). *Bumpy Black Holes in Alternate Theories of Gravity*. Phys. Rev. D, 83:104027.
- [138] Vincent, F. H., Meliani, Z., Grandclement, P., *et al.* (2016). *Imaging a boson star at the Galactic center*. Class. Quant. Grav., 33(10):105015.

- [139] Vincent, F. H., Meliani, Z., Grandclément, P., *et al.* (2016). *Imaging a boson star at the Galactic center*. Classical and Quantum Gravity, 33(10):105015. Publisher: IOP Publishing.
- [140] Wang, M., Guo, G., Yan, P., *et al.* (2023). *The ring shadow of rotating naked singularity with a complete photon sphere*.
- [141] Wheeler, J. A. (1955). *Geons*. Phys. Rev., 97:511–536.
- [142] Whiting, B. F. (1989). *Mode Stability of the Kerr Black Hole*. J. Math. Phys., 30:1301.
- [143] Yoshida, S. and Eriguchi, Y. (1997). *Rotating boson stars in general relativity*. Phys. Rev. D, 56:762–771.
- [144] Younsi, Z., Porth, O., Mizuno, Y., *et al.* (2020). *Modelling the polarised emission from black holes on event horizon-scales*. Proceedings of the International Astronomical Union, 14(S342):9–12.
- [145] Younsi, Z., Wu, K., and Fuerst, S. V. (2012). *General relativistic radiative transfer: formulation and emission from structured tori around black holes*. Astronomy & Astrophysics, 545:A13. Publisher: EDP Sciences.
- [146] Yuan, Y.-F., Narayan, R., and Rees, M. J. (2004). *Constraining Alternate Models of Black Holes: Type I X-Ray Bursts on Accreting Fermion-Fermion and Boson-Fermion Stars*. The Astrophysical Journal, 606(2):1112. Publisher: IOP Publishing.
- [147] Zerilli, F. J. (1970). *Effective potential for even parity Regge-Wheeler gravitational perturbation equations*. Phys. Rev. Lett., 24:737–738.